

An Unconditionally Time-Stable Level Set Method and Its Application to Shape and Topology Optimization

S.Y. Wang^{1,2}, K.M. Lim^{2,3}, B.C. Khoo^{2,3} and M.Y. Wang⁴

Abstract: The level set method is a numerical technique for simulating moving interfaces. In this paper, an unconditionally BIBO (Bounded-Input-Bounded-Output) time-stable consistent meshfree level set method is proposed and applied as a more effective approach to simultaneous shape and topology optimization. In the present level set method, the meshfree infinitely smooth inverse multiquadric Radial Basis Functions (RBFs) are employed to discretize the implicit level set function. A high level of smoothness of the level set function and accuracy of the solution to the Hamilton-Jacobi partial differential equation (PDE) can be achieved. The resulting dynamic system of coupled Ordinary Differential Equations (ODEs) is unconditionally positive definite, reinitialization free and BIBO time-stable. Significant advantages can be obtained in efficiency and accuracy over the standard finite difference-based level set methods. A moving superimposed finite element method is adopted to improve the accuracy in structural analysis and thus the physical model is consistent with the geometrical model. An explicit volume constraint approach is developed to satisfy the volume constraint function effectively and to guarantee the designs to be feasible during the level set evolution. Reinitialization is eliminated and nucleation of new holes is allowed for and the present nucleation mechanism can be physically meaningful. The final solution becomes less dependent on the initial designs. The

present method is applied to simultaneous shape and topology optimization problems and its success is illustrated.

Keyword: Level set method, radial basis functions, topology optimization, shape optimization, time stability, nucleation.

1 Introduction

The level set method first introduced by Osher and Sethian [Osher and Sethian (1988)] has become increasingly popular. It is a simple and versatile numerical technique for computing and analyzing the motion of an interface in two or three dimensions and following the evolution of interfaces. Since these interfaces may easily develop sharp corners, break apart, merge together and even disappear, the level set method has obtained a wide range of applications, including problems in fluid mechanics, combustion, solids modeling, computer animation, material science and image processing over the years [Sethian (1999); Osher and Fedkiw (2001, 2002); Osher and Paragios (2003); Tsai and Osher (2003)]. On the other hand, structural shape and topology optimization has become an effective design tool for obtaining more efficient structures in structural design [Wang and Wang (2004a); Wang and Zhou (2004); Tapp, Hansel, Mittelstedt, and Becker (2004); Wang and Wang (2006a); Zhou and Wang (2006); Wang, Tai, and Quek (2006); Cisilino (2007); Paris, Casteleiro, Navarrina, and Colominas (2007)]. A structural optimal topology can be reached by optimal modifications of holes and connectivities of the design domain [Akin and Arjona-Baez (2001); Bendsoe and Kikuchi (1988); Wang and Tai (2004)]. The topology optimization has the highest importance in the

¹ Corresponding author, Email: smaws@nus.edu.sg.

² Singapore-MIT Alliance, E4-04-10, 4 Engineering Drive 3, Singapore 117576.

³ Department of Mechanical Engineering, National University of Singapore, Singapore 119260.

⁴ Department of Mechanical and Automation Engineering, The Chinese University of Hong Kong, Shatin, NT, Hong Kong.

developing process of all structural optimization methods [Rozvany (2001a); Bendsøe and Kikuchi (1988); Xie and Steven (1993); Wang, Tai, and Wang (2006); Wang and Wang (2006a)]. The shape optimization changes the surface geometry in a manner that a homogenous stress distribution is achieved [Wang and Wang (2006c)]. Structural shape and topology optimization has been identified as one of the most challenging tasks in structural design [Bendsøe and Sigmund (2003)].

Recently, the level set methods have been applied to structural shape and topology optimization problems as an emerging family of methods based on the moving free boundaries [Sethian and Wiegmann (2000); Osher and Santosa (2001); Wang, Wang, and Guo (2003); Allaire, Jouve, and Toader (2004)]. Since both shape and topological changes in the structural design domain can be readily obtained by taking the voids as a phase and the free boundary as the dynamic interface, the level set methods can be applied to structural shape and topology optimization problems as a free boundary-based alternative to the popular element-based structural optimization methods [Rozvany (2001a)] such as the homogeneous approach first proposed by Bendsøe and Kikuchi [Bendsøe and Kikuchi (1988)] or its variant the SIMP (Solid Isotropic Microstructure with Penalization) method [Bendsøe (1989); Rozvany, Zhou, and Birker (1992)].

In shape and topology optimization using the level set methods, Sethian and Wiegmann (2000) [Sethian and Wiegmann (2000)] first extended the level set method of Osher and Sethian [Osher and Sethian (1988)] to capture the free boundary of a structure on a fixed Eulerian mesh. The von Mises equivalent stress, rather than the more suitable classical shape sensitivity analysis, was employed to improve the structural rigidity within the context of two-dimensional (2D) linear elasticity using the immersed interface method. Osher and Santosa [Osher and Santosa (2001)] investigated a two-phase optimization problem of a membrane modeled by a linear scalar partial differential equation. The free boundary was defined as the interface between two constituents occupying a given design domain. The level set

method was combined with the classical shape sensitivity analysis framework, but the linear or nonlinear elasticity was not included. Wang et al. [Wang, Wang, and Guo (2003)] implemented a level set method for structural topology optimization by establishing the velocity vector in terms of the shape of the boundary and the variational sensitivity as a physically meaningful link between the general structural topology optimization process and the universal level set methods. A smoothed Heaviside function was adopted in the finite element model and it was suggested that using the level set methods for structural topology optimization has the promising potentials in flexibility of handling topological changes, fidelity of boundary representation and degree of automation. Allaire et al. [Allaire, Jouve, and Toader (2004)] proposed an implementation of the level set methods for structural topology optimization where the front velocity during the optimization process was derived from the classical shape sensitivity analysis by using an adjoint problem and the front propagation was performed by solving the Hamilton-Jacobi equation. An artificial material model was used for the finite element analysis and it was illustrated that drastic topological changes during the structural optimization process were allowed for and the final design may be quite sensitive to the initial guess. More recently, many other researchers have further investigated shape and topology optimization using the level set methods, such as nucleation of new holes using topological derivatives [Allaire, Gournay, Jouve, and Toader (2004); Burger, Hackl, and Ring (2004); Wang, Mei, and Wang (2004); Allaire, de Gournay, Jouve, and Toader (2005); Hintermuller (2005); Amstutz and Andrá (2006)], or without using the Hamilton-Jacobi equation to update the level set function [Belytschko, Xiao, and Parimi (2003); Haber (2004); Guo, Zhao, and Wang (2005)], multi-material design [Wang and Wang (2004b, 2005b)], compliant mechanism design [Allaire, Jouve, and Toader (2004); Chen, Wang, Wang, and Xia (2005); Wang, Chen, Wang, and Mei (2005)], applications to vibration and multiple loads [Allaire and Jouve (2005)], as well as the introduction of radial basis functions for solving the Hamilton-Jacobi equation

[Cecil, Qian, and Osher (2004); Wang and Wang (2006b,c); Wang, Lim, Khoo, and Wang (2007)]. Despite the significant advances, there are still some fundamental issues to be resolved. In solving the structural shape and topology optimization problems, the standard level set methods [Osher and Santosa (2001); Wang, Wang, and Guo (2003); Allaire, Jouve, and Toader (2004); Wang and Wang (2004b, 2006a)] based on a finite difference method is known to be computationally expensive, slow to reach the convergence [Haber (2004)], easy to converge to a local minimum [Allaire, Jouve, and Toader (2004)], and even likely to converge to an infeasible solution when a volume constraint is imposed [Wang and Wang (2006a)]. In the standard level set methods, reinitialization has been widely used as a numerical remedy for maintaining stable evolution and ensuring desirable results [Sethian (1999); Osher and Fedkiw (2002)]. However, the reinitialization process can be quite complicated, expensive, even fraught with subtle side effects such as shift of the interface and ambiguous about when to reinitialize the level set function to a signed distance function [Li, Xu, Gu, and Fox (2005)]. To time advance the level set function, the timestep size must be sufficiently small to satisfy the Courant-Friedrichs-Lewy (CFL) condition for time stability due to the finite difference-based upwinding vanishing viscous schemes [Osher and Santosa (2001); Tsai and Osher (2003); Cecil, Qian, and Osher (2004)], resulting in a loss of computational efficiency in the standard level set methods. It was reported that the timestep size may not be strictly confined by the CFL condition in the work of [Kansa, Powerb, Fasshauerc, and Ling (2004); Platte and Driscoll (2005); Wang and Wang (2006b,c); Wang, Lim, Khoo, and Wang (2007)] due to the use of RBFs for time-dependent problems. Nevertheless, since time stability cannot be rigorously guaranteed, the use of large timesteps is not necessarily permitted and the computational cost may still be expensive. In addition to the computational efficiency, the existing level set methods may suffer from the computational accuracy. Most level set methods adopted an approximate smoothed Heaviside

step function in their physical models [Osher and Santosa (2001); Wang, Wang, and Guo (2003); Allaire, Jouve, and Toader (2004); Allaire and Jouve (2005); Wang and Wang (2004b, 2006b,c); Wang, Lim, Khoo, and Wang (2007)] and thus the distinct geometrical model represented by the level set function is inconsistent with the smeared or approximate physical model. This inconsistency may result in a low level of accuracy in the global and local responses such as displacements and strains in the finite element-based structural elasticity analysis, as shown in [Wang and Wang (2006a)]. In structural shape and topology optimization, an explicit volume constraint is usually adopted to limit the use of material [Bendsøe and Sigmund (2003)]. However, this volume constraint has not been appropriately resolved in the existing level set methods. In [Allaire, Jouve, and Toader (2002, 2004); Allaire, Gournay, Jouve, and Toader (2004); Allaire and Jouve (2005); Wang and Wang (2006b); Amstutz and Andrä (2006)], a fixed Lagrange multiplier was used during the course of evolution and thus only a relatively simple unconstrained optimization problem can be directly solved. In [Osher and Santosa (2001); Wang, Wang, and Guo (2003, 2004); Wang and Wang (2005b)], the variable Lagrange multiplier was derived from the fact that its shape derivative vanishes if the total material volume is conservative and keeps constant during the level set evolution. Since an explicit boundary integration of the strain energy density can be quite inaccurate due to the inconsistency of the geometrical and physical models, fluctuation of the structural volume can be significant [Wang, Wang, and Guo (2003, 2004); Wang and Wang (2005b)] during the iterations and infeasible designs may be evolved. A Newton's method was recommended to put the iteration back to the feasible set by Osher and Santosa [Osher and Santosa (2001)]. Prescribed multiplier values were used to push the total volume back to the desired volume during the evolution in the work of Wang and Wang [Wang and Wang (2006a)]. All these efforts cannot guarantee that the volume constraint be satisfied accurately during the iterations and thus the final solutions may be infeasible. In the standard level set methods, there is no

nucleation mechanism due to the maximum principle [Osher and Fedkiw (2002)] and therefore the final design is largely dependent on the initial guess, as noted by many researchers [Sethian (1999); Tsai and Osher (2003); Allaire, Gournay, Jouve, and Toader (2004); Burger, Hackl, and Ring (2004); Wang and Wang (2006b); Amstutz and Andrä (2006)]. Although some attempts have been made to incorporate both the topological derivatives and the shape derivatives into a level set model to resolve this problem [Burger, Hackl, and Ring (2004); Allaire, Gournay, Jouve, and Toader (2004); Wang and Wang (2006b); Amstutz and Andrä (2006)], it is known to be difficult to switch between the topological derivatives and the shape derivatives [Allaire, Gournay, Jouve, and Toader (2004); Wang, Mei, and Wang (2004)]. Hole nucleation may even be inconsistent with the popular regularization methods such as the perimeter control [Bendsøe (1995)] to ensure existence of solutions to the well-known ill-posed structural shape and topology optimization problems [Bendsøe and Sigmund (2003)]. Furthermore, it can be ambiguous about how to apply the topological derivatives based on infinitely small holes to the creation of new holes with sizes comparable to the finite element resolution [Allaire, Gournay, Jouve, and Toader (2004)]. As a whole, it could be concluded that the significant drawbacks of standard level set methods in efficiency and accuracy would greatly limit their further utility for structural shape and topology optimization.

The objective of this study is to propose an alternative efficient and accurate level set method for simultaneous shape and topology optimization. The infinitely smooth inverse multiquadric (IMQ) RBFs are used to discretize the implicit level set function. This meshfree discretization changes the original time dependent initial value problem into an interpolation problem. The resulting dynamic system is unconditionally positive definite, reinitialization-free and time stable. The use of relatively large timesteps is permitted and a rapid convergence to the final design in terms of total number of iterations can be achieved. A consistent physical model is de-

veloped based on a superimposed finite element method. The volume constraint can be satisfied accurately during the iterations by imposing the volume constraint in an explicit manner. Furthermore, a physically meaningful nucleation mechanism is naturally established without using topological derivatives due to the present extension velocities. The final design can thus become insensitive to the initial guess. Numerical examples are used to illustrate the distinct advantages of the present method in accuracy, efficiency, convergence speed and insensitivity to initial designs in shape and topology optimization of 2D problems that has been extensively studied in the literature [Wang, Wang, and Guo (2003); Allaire, Jouve, and Toader (2004); Allaire, Gournay, Jouve, and Toader (2004); Wang and Wang (2006a,b)].

2 An BIBO Time-Stable Level Set Method

2.1 A Level Set Evolution Model

The level set method first introduced by Osher and Sethian in 1988 [Osher and Sethian (1988)] has become popular recently for tracking, modeling and simulating the motion of dynamic interfaces (moving free boundaries) [Sethian (1999); Osher and Fedkiw (2002)]. The interface (or front) is closed, nonintersecting and represented implicitly through a smooth level set function $\Phi(\mathbf{x})$, and the interface itself is the zero isosurface or zero level set $\{\mathbf{x} \in \mathbb{R}^d \mid \Phi(\mathbf{x}) = 0\}$ ($d = 2$ or 3). Furthermore, $\Phi(\mathbf{x})$ has the following properties [Tsai and Osher (2003)]:

$$\begin{aligned} \Phi(\mathbf{x}) &= 0 & \forall \mathbf{x} \in \partial\Omega \cap D \\ \Phi(\mathbf{x}) &< 0 & \forall \mathbf{x} \in \Omega \setminus \partial\Omega \\ \Phi(\mathbf{x}) &> 0 & \forall \mathbf{x} \in (D \setminus \Omega) \end{aligned} \quad (1)$$

where $D \subset \mathbb{R}^d$ is a fixed design domain in which all admissible shapes Ω are included, i.e. $\Omega \subset D$. In the level set model, the local unit normal n can be given by

$$n = \frac{\nabla\Phi}{|\nabla\Phi|} \quad (2)$$

and the volume integral of a function $F(\mathbf{x})$ is defined as

$$\int_D F(\mathbf{x}) H(-\Phi) d\Omega \quad (3)$$

where $H(\Phi)$ is the Heaviside step function. Hence, the volume $V(\Phi)$ can be expressed as

$$V(\Phi) = \int_D H(-\Phi) d\Omega \quad (4)$$

To let the level set function dynamically change with time, a continuous velocity field $v(\mathbf{x})$ should be introduced and the level set evolution can be obtained by solving the following Hamilton-Jacobi equation [Sethian (1999); Osher and Fedkiw (2002)]:

$$\frac{\partial \Phi}{\partial t} + v_n |\nabla \Phi| = 0, \quad \Phi(\mathbf{x}, 0) = \Phi_0(\mathbf{x}) \quad (5)$$

where

$$v_n = v \cdot n = v \cdot \frac{\nabla \Phi}{|\nabla \Phi|} \quad (6)$$

and t is the pseudo-time, $\Phi_0(\mathbf{x})$ embeds the initial position of the interface. This first-order nonlinear hyperbolic PDE (5) can be solved numerically by introducing spatial and temporal discretizations appropriately [Sethian (1999); Osher and Fedkiw (2002)]. In the standard level set methods [Sethian (1999); Osher and Fedkiw (2002); Wang, Wang, and Guo (2003); Allaire, Jouve, and Toader (2004); Wang and Wang (2004b)], the finite difference method is used to perform the spatial discretizations, but the computational cost may become expensive [Haber (2004); Wang and Wang (2006c)] in terms of the total number of iterations due to the CFL condition for time stability. In the present study, an alternative level set method is presented based on the RBF meshfree discretization. The implicit level set function is discretized by the infinitely smooth inverse multiquadric RBFs. Reinitialization is eliminated and time stability can be guaranteed during the level set evolution. The computational efficiency can thus be significantly improved due to the permitted use of large timesteps. The accuracy can be maintained due to the use of a consistent physical model. The present time-stable meshfree level set method is to be discussed in detail in the following sections.

2.2 Radial Basis Functions

Radial basis functions (RBFs) are radially-symmetric functions centered at knots [Morse,

Yoo, Chen, Rheingans, and Subramanian (2001)], or particular points, which can be expressed as follows:

$$\varphi_i(\mathbf{x}) = \varphi(\|\mathbf{x} - \mathbf{x}_i\|), \quad \mathbf{x}_i \in D \quad (7)$$

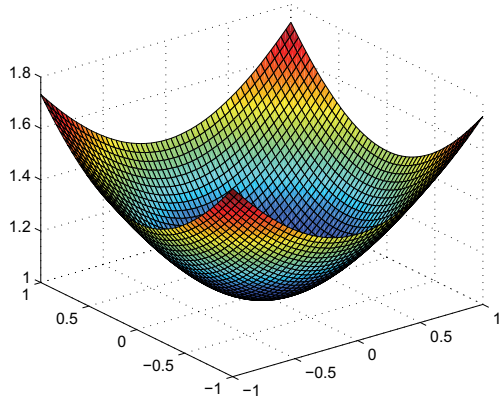
where $\|\cdot\|$ denotes the Euclidean norm on \mathbb{R}^d [Cheng, Golberg, Kansa, and Zammito (2003)], φ_i the i -th radial basis function, and \mathbf{x}_i the position of the i -th knot. A single fixed function form $\varphi : \mathbb{R}^+ \rightarrow \mathbb{R}$ with $\varphi(0) \geq 0$ is used as the basis to form a family of independent RBFs. There is a large class of possible RBFs, but only a few of them are commonly used, such as thin-plate splines, polyharmonic splines, Sobolev splines, Gaussians, multiquadric (MQ) splines and compactly supported RBFs [Cheng, Golberg, Kansa, and Zammito (2003); Kansa, Powerb, Fasshauerc, and Ling (2004); Wang and Wang (2006b)]. Among them, the MQ splines, or multiquadrics (MQs), have been widely used [Cheng, Golberg, Kansa, and Zammito (2003); Kansa, Powerb, Fasshauerc, and Ling (2004)], which can be written as

$$\varphi_i(\mathbf{x}) = \sqrt{(\mathbf{x} - \mathbf{x}_i)^2 + c_i^2} \quad (8)$$

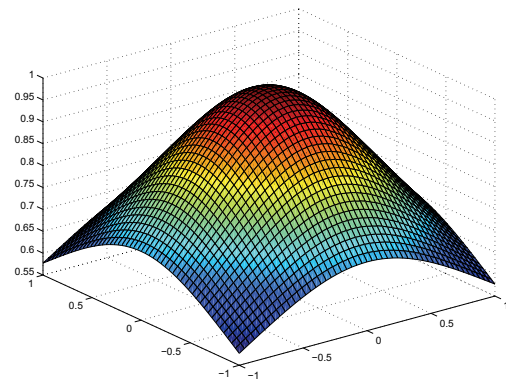
where c_i ($c_i > 0$) is a free shape parameter, which is commonly assumed to be a constant for all i in most applications [Cheng, Golberg, Kansa, and Zammito (2003)]. However, the MQs are only conditionally positive definite [Cheng, Golberg, Kansa, and Zammito (2003)] and have to be augmented by a leading constant term in the series and higher-order MQs require more terms in the polynomial [Schaback and Wendland (2001)]. As a comparison, the inverse multiquadric (IMQ) splines, which can be expressed as

$$\varphi_i(\mathbf{x}) = \frac{1}{\sqrt{(\mathbf{x} - \mathbf{x}_i)^2 + c_i^2}} \quad (9)$$

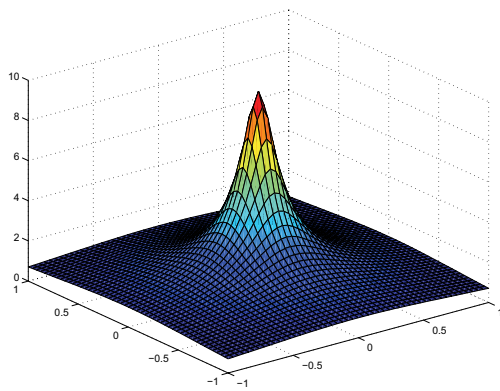
are positive definite [Cheng, Golberg, Kansa, and Zammito (2003)] and can thus be used without augmentation. In the present study, for the purpose of numerical convenience, the IMQ spline shown in Eq. (9) is adopted to develop a time-stable meshfree level set method. Figure 1 displays the shapes of multiquadric and inverse multiquadric splines centered at the original point.



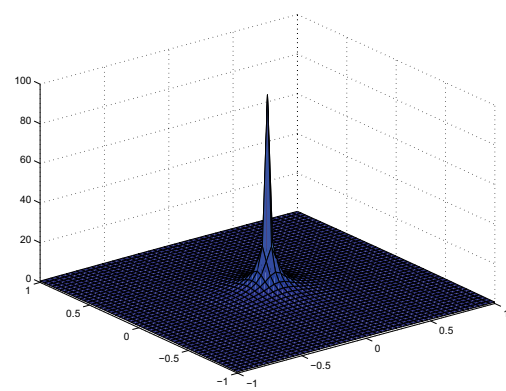
(a) Multiquadrics ($c = 1$)



(b) Inverse multiquadrics ($c = 1$)



(c) Inverse multiquadrics ($c = 0.1$)



(d) Inverse multiquadrics ($c = 0.01$)

Figure 1: Infinitely smooth RBF splines with a free shape parameter.

These splines are infinitely smooth since they are continuously differentiable [Kansa, Powerb, Fasshauerc, and Ling (2004)], as shown in Eqs. (8) and (9). It can be seen that a larger free shape parameter will result in a flatter shape of the inverse multiquadric spline, which is less sensitive to the difference in radial distance. According to the observations made in [Kansa, Powerb, Fasshauerc, and Ling (2004)], more accurate solutions may be obtained when the parameter c gets larger until it reaches the breakdown point caused by the machine roundoff error. Hence, appropriate choice of the shape parameter can be of significant importance when using the infinitely smooth splines. In the present study, the shape parameter is obtained by a trial and error procedure.

2.3 RBF Discretization of the Level Set Function

The time dependent level set function $\Phi(\mathbf{x}, t)$ can be discretized by the IMQ RBFs as shown in Eq. (8) with N knots by using N IMQ splines centered at these knots. The resulting RBF discretization of the level set function can be written as follows:

$$\Phi = \Phi(\mathbf{x}, t) = \sum_{i=1}^N \alpha_i(t) \varphi_i(\mathbf{x}) \quad (10)$$

where $\alpha_i(t)$ is the time dependent expansion coefficient of the IMQ spline positioned at the i -th knot. The RBF discretization in Eq. (10) can be further given in compact form as

$$\Phi(\mathbf{x}, t) = \boldsymbol{\Phi}^T(\mathbf{x}) \boldsymbol{\alpha}(t) \quad (11)$$

where

$$\boldsymbol{\Phi}(\mathbf{x}) = [\varphi_1(\mathbf{x}) \quad \cdots \quad \varphi_N(\mathbf{x})]^T \in \mathbb{R}^{N \times 1} \quad (12)$$

$$\boldsymbol{\alpha}(t) = [\alpha_1(t) \quad \cdots \quad \alpha_N(t)]^T \in \mathbb{R}^{N \times 1} \quad (13)$$

It should be noted that in (11) only the generalized RBF expansion coefficient $\boldsymbol{\alpha}(t)$ is explicitly time dependent and thus all the time dependence in the present RBF discretization is due to the generalized expansion coefficients and all the knots are fixed in space. Since the IMQ RBFs are infinitely smooth [Kansa, Powerb, Fasshauerc, and Ling (2004)], the discretized level set function will also be infinitely smooth and thus a

high level of smoothness of the level set function can be achieved due to the present RBF discretization. Furthermore, since a mesh or grid is not needed in this RBF discretization, the present level set method based on the IMQ RBFs is mesh-free. With this meshfree discretization, the first-order spatial derivatives of the level set function in the Hamilton-Jacobi equation (5) can be readily obtained and a discretized governing equation of motion of the level set function can thus be derived.

2.4 Governing Equation of Motion

Substituting Eq. (11) into the Hamilton-Jacobi PDE (5) yields the following ODE:

$$\boldsymbol{\Phi}^T \frac{d\boldsymbol{\alpha}}{dt} + v_n |(\nabla \Phi)^T \boldsymbol{\alpha}| = 0 \quad (14)$$

where

$$|(\nabla \Phi)^T \boldsymbol{\alpha}| = \left[\left(\frac{\partial \boldsymbol{\Phi}^T}{\partial x} \boldsymbol{\alpha} \right)^2 + \left(\frac{\partial \boldsymbol{\Phi}^T}{\partial y} \boldsymbol{\alpha} \right)^2 + \left(\frac{\partial \boldsymbol{\Phi}^T}{\partial z} \boldsymbol{\alpha} \right)^2 \right]^{1/2} \quad (15)$$

$$\frac{\partial \boldsymbol{\Phi}}{\partial x} = \left[\frac{\partial \varphi_1}{\partial x} \quad \cdots \quad \frac{\partial \varphi_N}{\partial x} \right]^T \in \mathbb{R}^{N \times 1} \quad (16)$$

$$\frac{\partial \boldsymbol{\Phi}}{\partial y} = \left[\frac{\partial \varphi_1}{\partial y} \quad \cdots \quad \frac{\partial \varphi_N}{\partial y} \right]^T \in \mathbb{R}^{N \times 1} \quad (17)$$

$$\frac{\partial \boldsymbol{\Phi}}{\partial z} = \left[\frac{\partial \varphi_1}{\partial z} \quad \cdots \quad \frac{\partial \varphi_N}{\partial z} \right]^T \in \mathbb{R}^{N \times 1} \quad (18)$$

$$\frac{\partial \varphi_i}{\partial x} = \frac{x - x_i}{((x - x_i)^2 + (y - y_i)^2 + (z - z_i)^2 + c_i^2)^{3/2}} \quad (19)$$

$$\frac{\partial \varphi_i}{\partial y} = \frac{y - y_i}{((x - x_i)^2 + (y - y_i)^2 + (z - z_i)^2 + c_i^2)^{3/2}} \quad (20)$$

$$\frac{\partial \varphi_i}{\partial z} = - \frac{z - z_i}{((x - x_i)^2 + (y - y_i)^2 + (z - z_i)^2 + c_i^2)^{3/2}} \quad (21)$$

It should be noted that a smooth evolution can be guaranteed since the norm of the gradients of the discretized level set function can also be infinitely smooth and continuously differentiable, significantly different from the finite difference-based upwind schemes [Sethian (1999); Osher and Fedkiw (2002)]. At the initial time, all the time dependent variables $\boldsymbol{\alpha}(t)$ in (14) should be pre-specified. This initial value problem can be considered equivalent to an interpolation problem since the expansion coefficients $\boldsymbol{\alpha}(t)$ at the initial time are found as a solution of the interpolation problem [Wang and Wang (2006b)]. Hence, the preliminary starting point of the use of RBFs to solve PDEs is the interpolation problem that is equivalent to solving the initial value problem. The original time-dependent initial value problem defined by the Hamilton-Jacobi PDE (5) is thus discretized into a time-dependent interpolation problem for the initial values of the generalized expansion coefficients $\boldsymbol{\alpha}(t)$, as shown in Eq. (14), which governs the motion of the moving free boundary $\Phi(\mathbf{x}, t) = 0$.

To time advance the initial values of $\boldsymbol{\alpha}(t)$ in the governing equation of motion (14), a collocation formulation of the method of lines is presented because of its inherent simplicity. The governing equation of motion (14) is extended to the whole design domain D and the normal velocities v_n at the front are thus replaced by the extension velocities v_n^e . Based on the principle of collocation method, all nodes for the spatial discretization of the extended ODE (14) are located sequentially at the spatially fixed knots of the IMQ RBFs. Furthermore, in the present implementation, for the purpose of simplicity, all the nodes of a fixed mesh for structural analysis are taken as the fixed knots, though not necessary. Using the present collocation method for the N knots, a set of resulting ODEs can be compactly written as follows:

$$\mathbf{H} \frac{d\boldsymbol{\alpha}}{dt} + \mathbf{b}(\boldsymbol{\alpha}) = 0 \quad (22)$$

where

$$\mathbf{H} = \begin{bmatrix} \varphi_1(\mathbf{x}_1) & \cdots & \varphi_N(\mathbf{x}_1) \\ \vdots & \ddots & \vdots \\ \varphi_1(\mathbf{x}_N) & \cdots & \varphi_N(\mathbf{x}_N) \end{bmatrix} \in \mathbb{R}^{N \times N} \quad (23)$$

$$\mathbf{b}(\boldsymbol{\alpha}) = \begin{bmatrix} v_n^e(\mathbf{x}_1) |(\nabla \Phi^T(\mathbf{x}_1)) \boldsymbol{\alpha}| \\ \vdots \\ v_n^e(\mathbf{x}_N) |(\nabla \Phi^T(\mathbf{x}_N)) \boldsymbol{\alpha}| \end{bmatrix} \in \mathbb{R}^{N \times 1} \quad (24)$$

Since the inverse multiquadric collocation matrix \mathbf{H} is unconditionally positive definite and theoretically invertible [Micchelli (1986); Buhmann (2004); Kansa, Powerb, Fasshauerc, and Ling (2004)], the resulting ODE system (22) is solvable and nonsingular. Equation (22) can be regarded as a collocation formulation of the general method of lines [Madsen (1975)], in which a time dependent PDE problem is reduced to a simpler time dependent ODE problem by discretization.

The set of coupled non-linear ODEs of Eq. (22) can be solved by several well-established ODE solvers such as the first-order forward Euler's method and higher-order Runge-Kutta, Runge-Kutta-Fehlberg, Adams-Bashforth, or Adams-Moulton methods [Greenberg (1998)]. In the present study, only the first-order forward Euler's method is used since it is the simplest solution algorithm for ODE initial condition problems and often used for comparison with more accurate algorithms, which are more complex and tedious to implement. Using Euler's method, an approximate solution to Eq. (22) can be given by

$$\boldsymbol{\alpha}(t^{n+1}) = \boldsymbol{\alpha}(t^n) - \tau \mathbf{H}^{-1} \mathbf{b}(\boldsymbol{\alpha}(t^n)) \quad (25)$$

where τ is the timestep size. Because of the fixed location of the RBF knots, the inverse multiquadric collocation matrix \mathbf{H} is time independent and storing the initial value of its inverse matrix will save the computational cost. Hence, the use of the inverse matrix may not cause an overly severe problem during the level set evolution. Furthermore, the dense collocation matrix \mathbf{H} can be effectively handled by several existing iterative methods [Buhmann (2004)]. Compared with the popular finite difference-based upwind schemes [Osher and Fedkiw (2002)], the present method may require more computational effort at

a single time step, however, this drawback can be significantly eliminated and the present meshfree method may even be computationally more effective and attractive in terms of total number of iterations due to its distinctive properties such as reinitialization-free evolution and BIBO time stability, which will be next discussed in detail.

2.5 Reinitialization-free Evolution

In the standard finite difference-based level set methods, it is well known that in many situations the level set function may develop flat and/or steep gradients at the front, leading to problems in numerical approximations [Peng, Merriman, Osher, Zhao, and Kang (1999); Tsai and Osher (2003)]. To cope with these problems, a reinitialization procedure is periodically performed to resurrect the behavior of the level set function in the neighborhood of the front, while keeping the zero location unchanged. The reinitialization process can be complicated to implement, expensive in CPU time and even fraught with subtle side effects [Li, Xu, Gu, and Fox (2005); Marchandise, Remacle, and Chevaugeon (2006)].

In the present global approximation method using RBF implicit modeling for the level set function, the occurrence of a flat level set function in the neighborhood of the front can be virtually prevented due to the global interpolation using RBFs. The parametrization using IMQ RBFs with global support makes the level set function and its gradients at any point dependent on each knot value in the whole design domain D , rather than the neighboring knot values only, different from the finite difference-based upwind schemes [Sethian (1999); Osher and Fedkiw (2002)]. According to Eqs. (15)-(21), during the course of evolution it can be generally maintained that

$$|\nabla\Phi| = |(\nabla\phi)^T \alpha| \neq 0 \quad (26)$$

provided that there are some non-flat knot values existing in the whole domain D . Hence, a flat surface is unlikely to be evolved due to the globally supported RBFs and a smooth level set evolution can thus be achieved. It should be noted that in the literature [van den Doel and Ascher (2006)] non-local functionals were used to obtain almost

smooth level set evolution through a regularization method without reinitialization, but radial basis functions were not considered. Furthermore, since the gradients can be readily obtained from (15) to (21), steep gradients will not cause serious numerical approximation problems, different from the finite difference method. More importantly, the magnitude of the gradients can be scaled down without changing the location of the moving free boundary $\Phi(\mathbf{x}, t) = 0$. According to the present RBF discretization (11) of the implicit level set function, the generalized expansion coefficients α can be normalized without changing the zero location $\Phi(\mathbf{x}, t) = 0$ as follows:

$$\Phi(\mathbf{x}, t) = \phi^T(\mathbf{x})\alpha(t) = \phi^T(\mathbf{x})(\alpha(t)/C) = 0 \quad (27)$$

where C ($C \geq 1$) is a constant used to normalize α . Hence, according to Eq. (15), the magnitude of the norm of the gradients can also be scaled down by $1/C$.

Therefore, in the present level set method, reinitialization becomes unnecessary and can be eliminated in the numerical analysis procedure in solving the coupled ODEs (22). The present method becomes reinitialization-free and the computational cost can be reduced. It should also be noted that in the recent literature [Ye, Bresler, and Moulin (2002); Leito and Scherzer (2003); Haber (2004); Li, Xu, Gu, and Fox (2005); van den Doel and Ascher (2006)], many level set methods without reinitialization have been proposed and the level set function is well maintained as a signed distance function during the evolution. In the present study, the global support radial basis functions are used to prevent the concurrence of flat level sets and to maintain the behavior of the level set function at the front without reinitialization. Although the level set function is initialized as a signed distance function, no special effort is made to keep this property during the course of evolution, which will lead to nucleation of new holes in the material domain, as further discussed later.

2.6 BIBO Time Stability

In the standard finite difference-based level set methods, explicit time marching schemes are usu-

ally used and the timesteps must be sufficiently small to achieve the time stability due to the CFL condition in the von Neumann sense [Osher and Fedkiw (2002)] in achieving the monotony while solving the vanishing viscous Hamilton-Jacobi equation. The CFL condition states that a necessary condition for the convergence of an explicit finite difference time marching scheme is that the domain of dependence of the discrete problem includes the domain of dependence of the differential equation in the limit as the length of the finite difference steps goes to zero. The CFL condition is only a necessary time stability condition, not sufficient. In the present study, time stability is achieved by ensuring that the numerical solution to (22) remains bounded at any time, rather than monotonically decaying with time. It should be noted that the monotonically decaying system guaranteed by the CFL condition in the finite difference-based upwind schemes [Sethian (1999); Osher and Fedkiw (2002)] may generate a flat level set function and the periodic reinitialization may introduce significant external errors to destroy the time stability.

As shown in Eq. (27), the generalized expansion coefficients α can be normalized without changing the zero location. We can choose $C = |\alpha|$ such that we have $|\alpha| = 1$ after normalization at each step, which will make the solution α always bounded. Generally, a system has bounded solutions if for each initial condition x_0 there is a constant B such that for all $t \geq 0$,

$$\|x(t)\| \leq B \quad (28)$$

where $x(t)$ is the solution with $x(0) = x_0$. Hence, the ODE dynamic system (22) has a bounded solution for all initial conditions and can thus be Lyapunov stable [Bhatia and Szego (1970)] provided that the input the extension velocities are bounded. The present dynamic system can thus be kept BIBO stable. The normalization is performed at each iteration and thus the solution α will never diverge to infinity due to the BIBO time stability. As aforementioned, a flat level set function will not occur due to the present global interpolation using RBFs and thus will not be affected by this normalization technique. This is a significant advantage of the present meshfree level set

method over the standard level set methods using local interpolation methods. The use of large timesteps can be permitted and drastic reduction in computational cost in terms of total number of iterations over the standard level set methods can be obtained, as illustrated in the present numerical examples. It should be noted that the present handling on time stability circumvents the numerical difficulty in complex eigenvalue analysis usually involved in linear time stability analysis of a time-dependent system [Platte and Driscoll (2005)] and can thus be computationally efficient.

2.7 Consistent Physical Model

In the standard level set methods, an Eulerian approach in which the design domain D is uniformly meshed is usually adopted [Wang and Wang (2006a)]. The topological changes are easy to handle and remeshing is not needed while the free boundary can still be captured. However, the distinct Heaviside function in (3) is approximated as a smoothed Heaviside function to perform the volume integration [Osher and Santosa (2001); Wang, Wang, and Guo (2003); Allaire, Jouve, and Toader (2004); Allaire and Jouve (2005); Wang and Wang (2004b, 2006a,b)] and thus the physical model is inconsistent with the geometrical model. Without remeshing, the free boundary is actually smeared in the physical model and the computational inaccuracy problem may arise. The convergence of this fictitious domain analysis can be obtained in the limit of mesh refinement [Norato, Haber, Tortorelli, and Bendsøe (2004)], but the computational cost would become too expensive.

In the present study, the moving superimposed finite element method (S-FEM) previously developed by the authors [Wang and Wang (2006a)] is adopted to make the physical model consistent with the distinct geometric model represented by the level set method as shown in Eq. (1). The basic idea of this method is to construct the adaptive local mesh around the captured free boundary and to superimpose the moving local mesh onto the fixed global mesh properly. Figure 2 shows the S-FEM model for a design with a central hole, in which a fixed Eulerian mesh is used as a global mesh, and an independently constructed local FE

mesh with triangular elements around the boundary of the central hole in the local domain $\Omega^L \subset D$ with the boundary Γ^L is superimposed onto the global mesh. It is also defined that $\Omega^G = D \setminus \Omega^L$ and the boundary between Ω^G and Ω^L is $\Gamma^{GL} = \Gamma^L \setminus (\partial\Omega \cap \Gamma^L)$. More details of this method can be found in [Wang and Wang (2006a)]. Based on this configuration of mesh superimposition, the labor intensive efforts in mesh generation can be greatly reduced [Wang and Wang (2006a)] and the physical model is consistent with the geometrical model. The computational accuracy in global and local responses can be significantly improved, as noted in [Wang and Wang (2006a)].

It should be noted that iterative equation solvers were recommended by a number of researchers [Fish and Guttal (1996); Okada, Liu, Ninomiya, Fukui, and Kumazara (2004); Wang and Wang (2006a)] to expediate the equation solving process. However, due to the moving free boundary, the global stiffness matrix may become quite near singular and thus an iterative solver may fail to find a solution. In the present study, only a linear sparse direct solver LDLT is used to ensure that a solution can always be obtained during the level set evolution, though the computational cost may become higher. In the present S-FEM model, the computational cost can be reduced by eliminating all the degrees of freedom associated with the nodes in the void domain. Since the present physical model is consistent, the free boundary can be modeled accurately and the popular weak material model for the void phase [Sigmund (2001); Bendsøe and Sigmund (2003); Wang, Wang, and Guo (2003); Allaire, Jouve, and Toader (2004); Wang and Wang (2006a,b)] is not needed.

3 Shape and Topology Optimization Using the Level Set Method

3.1 Minimum Compliance Design

In the classical shape and topology optimization problems, the minimum compliance design has been widely investigated by the popular topology optimization methods such as the homogenization method [Bendsøe and Kikuchi (1988)] and the evolutionary structural optimization method [Xie

and Steven (1993)].

Using a level set representation model as shown in Eq. (1) and the volume integration formula (3), the standard notion of a classical minimum compliance design problem in [Sigmund (2001); Bendsøe and Sigmund (2003)] can be re-written as follows:

$$\begin{aligned} \min_{\Phi} \quad & J(\mathbf{u}, \Phi) = \int_D (\boldsymbol{\varepsilon}(\mathbf{u}))^T \mathbf{C} \boldsymbol{\varepsilon}(\mathbf{u}) H(-\Phi) d\Omega \\ \text{s.t.} \quad & a(\mathbf{u}, \mathbf{v}, \Phi) = L(\mathbf{v}, \Phi), \mathbf{u}|_{\Gamma_D} = \mathbf{u}_0, \forall \mathbf{v} \in U \\ & V(\Phi)/V_0 = \zeta \end{aligned} \quad (29)$$

where $J(\mathbf{u}, \Phi)$ is the objective function, \mathbf{u} the displacement field, $\boldsymbol{\varepsilon}$ the strain field, \mathbf{C} the Hook elasticity tensor, $V(\Phi)$ the material volume as defined in Eq. (4), V_0 the design domain volume and ζ the prescribed volume fraction. The linearly elastic equilibrium equation is written in its weak variational form in terms of the energy bilinear form $a(\mathbf{u}, \mathbf{v}, \Phi)$ and the load linear form $L(\mathbf{v}, \Phi)$ [Bendsøe and Sigmund (2003)], with \mathbf{v} denoting a virtual displacement field in the space U of kinematically admissible displacement fields, and \mathbf{u}_0 the prescribed displacement on the admissible Dirichlet boundary Γ_D .

The Lagrange multiplier method can be used to solve the optimization problem (29) [Osher and Santosa (2001)]. By setting the constraint on the equilibrium state inactive, the Lagrangian $\mathcal{L}(\mathbf{u}, \Phi, \ell)$ with a Lagrange multiplier ℓ can be given by

$$\mathcal{L}(\mathbf{u}, \Phi, \ell) = J(\mathbf{u}, \Phi) + \ell G(\Phi) \quad (30)$$

where the constraint functional $G(\Phi)$ can be expressed as

$$G(\Phi) = V(\Phi) - \zeta V_0 = 0 \quad (31)$$

It should be noted that the displacement field \mathbf{u} is also a function of Φ , i.e. $\mathbf{u} = \mathbf{u}(\Phi)$. According to the Kuhn-Tucker condition of the optimization, the necessary condition for a minimizer is

$$D_{\Phi} \mathcal{L}(\mathbf{u}(\Phi), \Phi, \ell) = 0 \quad (32)$$

where $D_{\Phi} \mathcal{L}(\mathbf{u}(\Phi), \Phi, \ell)$ is the gradient of the Lagrangian with respect to Φ .

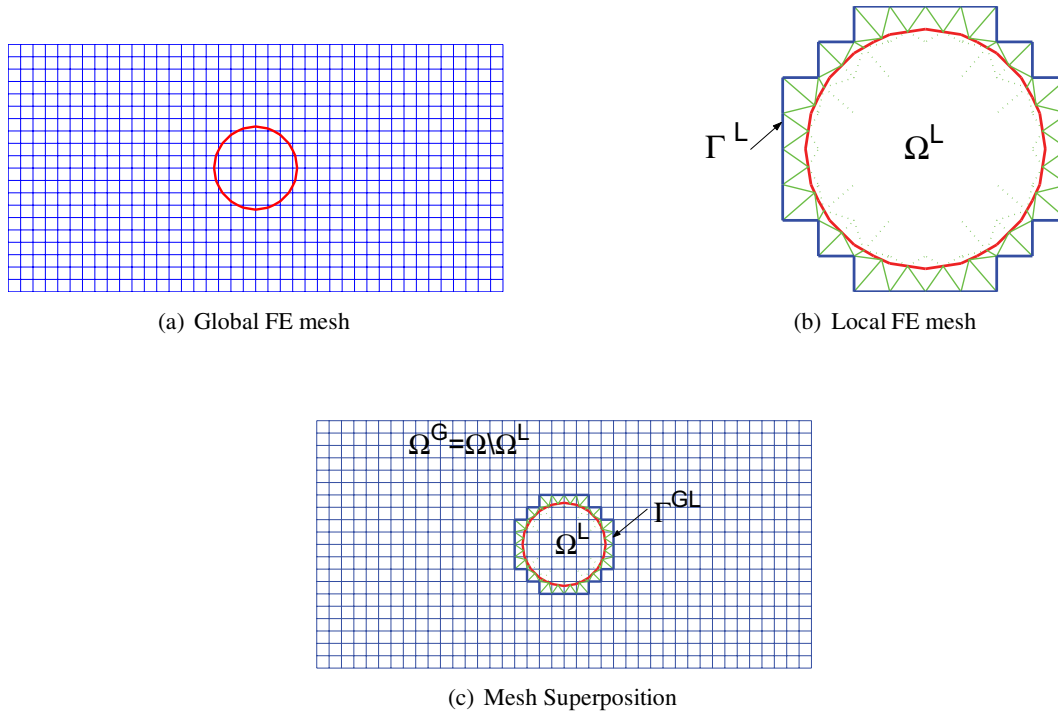


Figure 2: The S-FEM model.

3.2 Shape Derivatives

The gradient of the Lagrangian $D_{\Phi} \mathcal{L}(\mathbf{u}(\Phi), \Phi, \ell)$ may be obtained in a number of different ways following the well-known approach of Murat and Simon of shape diffeomorphism [Sokolowski and Zolesio (1992)]. In the present study, the shape sensitivity analysis presented by Allaire et al. [Allaire, Jouve, and Toader (2004)] is adopted to derive the time-dependent shape derivatives.

Usually, the boundary ∂D of the whole structural shape and topology design domain D can be decomposed [Allaire, Jouve, and Toader (2004)] as

$$\partial D = \partial D_D \cup \partial D_N \cup \partial D_H \quad (33)$$

where ∂D_D is the Dirichlet boundary, ∂D_N the non-homogeneous Neumann boundary, and ∂D_H the homogeneous Neumann boundary (traction free). To derive the shape derivatives from the classical shape sensitivity analysis [Sokolowski and Zolesio (1992)], it is assumed that the shape boundary $\partial \Omega$ of an admissible design Ω can satisfy the following conditions:

isfy the following conditions:

$$\partial \Omega = \Gamma_D \cup \Gamma_N, \quad \Gamma_D \subset \partial D_D, \quad \Gamma_N = \partial D_N \cup \Gamma_H \quad (34)$$

where Γ_D is the admissible Dirichlet boundary, Γ_N the Neumann boundary, and Γ_H the homogeneous Neumann boundary. Furthermore, it is assumed that the surface loads are design independent and applied only on a fixed subset of the boundary Γ_N and the Dirichlet boundary Γ_D is with zero displacements. In the present shape and topology optimization, only part of the traction free homogeneous Neumann boundary $\Gamma_M \in \Gamma_H$ is initially chosen to be optimized as the moving free boundary, which is represented by the dynamic interface $\Phi(\mathbf{x}) = 0$ in the present level set model.

Based on local perturbations of the moving free boundary of an admissible design Ω [Allaire, Jouve, and Toader (2004)], the resulting shape derivative of the Lagrangian can be written as

$$\frac{d\mathcal{L}}{dt} = \int_{\Gamma_M} (\ell - \boldsymbol{\varepsilon}^T \mathbf{C} \boldsymbol{\varepsilon}) v_n ds \quad (35)$$

where v_n is the normal velocity at the moving free boundary Γ_M . Furthermore, the resulting

shape derivative of the volume constraint functional $G(\Phi)$ (31) can be expressed as

$$\frac{dG}{dt} = \int_{\Gamma_M} v_n ds \quad (36)$$

Hence, these time-dependent shape derivatives can be obtained from a surface integration. In a level set method, only the normal velocity field v_n associated with the physical model is needed during the level set evolution and thus it is unnecessary to perform an explicit surface integration. In the present shape and topology optimization, choosing the normal velocity field v_n is equivalent to choosing a descent direction for the objective function, which can be easily implemented by using a steepest gradient method [Osher and Santosa (2001); Wang, Wang, and Guo (2003); Allaire, Jouve, and Toader (2004)].

According to the shape derivative in Eq. (35), a descent direction of the normal velocity v_n for the Lagrangian can be obtained by simply identifying the normal velocity v_n as

$$v_n = \boldsymbol{\varepsilon}^T \mathbf{C} \boldsymbol{\varepsilon} - \ell \quad (37)$$

in which the normal velocity v_n at the moving free boundary Γ_M can be determined by the strain energy density and a Lagrange multiplier. Hence, the normal velocity field is linked with the objective function and physics of the present minimum compliance design problem. The variable Lagrange multiplier ℓ can be obtained by using the proposed explicit volume constraint handling approach as follows.

3.3 Explicit Volume Constraint Handling Approach

An explicit volume constraint handling approach is developed since the approaches available in the literature [Osher and Santosa (2001); Wang, Wang, and Guo (2003); Wang and Wang (2006a)] to handle the volume constraint in Eq. (31) to obtain the Lagrange multiplier may become quite ineffective to keep the design feasible during the level set evolution. These approaches [Osher and Santosa (2001); Wang, Wang, and Guo (2003); Wang and Wang (2006a)] were actually based on an implicit constraint on the volume function

$V(\Phi)$. To keep all the designs feasible, the volume constraint in (31) must be satisfied accurately during the level set evolution. Hence, at any time we have $V(\Phi) = \zeta V_0$. Since the total material volume $V(\Phi)$ is required to be conservative, its time derivative vanishes, i.e.,

$$\frac{dV}{dt} = \frac{dG}{dt} = \int_{\Gamma_M} v_n ds = 0 \quad (38)$$

Based on this implicit constraint on the volume function $V(\Phi)$, the Lagrange multiplier ℓ can be obtained, as shown in [Osher and Santosa (2001); Wang, Wang, and Guo (2003); Wang and Wang (2006a)]. Substituting Eq. (37) into Eq. (38) yields the Lagrange multiplier ℓ as

$$\ell = \frac{\int_{\Gamma_M} \boldsymbol{\varepsilon}^T \mathbf{C} \boldsymbol{\varepsilon} ds}{\int_{\Gamma_M} ds} \quad (39)$$

However, this volume constraint handling approach has several drawbacks. Since the desired volume is not used directly, this implicit handling approach requires that the initial design satisfy the volume constraint exactly. Furthermore, there is no guarantee that the volume keep unchanged during the iterations due to the errors involved. The Lagrange multiplier may be inaccurately estimated due to the boundary integrations. The inconsistent physical models [Wang, Wang, and Guo (2003); Allaire, Jouve, and Toader (2004)] adopted a smoothed Heaviside function to approximate the moving free boundary. The strain energy density at the boundary is calculated with a low level of accuracy due to the averaging effect. The total volume thus tends to drift to the infeasible set during the evolution. Osher and Santosa [Osher and Santosa (2001)] used a Newton's method to put the iteration back to the feasible set when the volume drifts too far away. Wang and Wang [Wang and Wang (2006a)] used a prescribed multiplier value to push the total volume back to the desired volume during the evolution. All these additional efforts cannot guarantee the volume constraint to be satisfied accurately during the iterations and thus the final solutions may be infeasible.

In the present explicit volume constraint handling approach, it is only required that the volume constraint be explicitly satisfied at the end of each time step, i.e.,

$$G(\Phi(t^n + \tau)) = 0 \quad (40)$$

Hence, according to Eq. (31), we have

$$V(\Phi(t^n + \tau)) = \zeta V_0 \quad (41)$$

According to Eq. (4), the volume $V(\Phi(t^n + \tau))$ can be obtained if the implicit level set function in Eq. (11) is updated as $\Phi(t^n + \tau)$, which can be written as

$$\Phi(t^n + \tau) = \phi^T \alpha(t^n + \tau) \quad (42)$$

where $\alpha(t^n + \tau)$ can be obtained from Eq. (25) and it turns out to be a function of the Lagrange multiplier ℓ when the normal velocity v_n in Eq. (37) and the extension velocity v_n^e later discussed are adopted to calculate \mathbf{b} in Eq. (24). Hence, $V(\Phi(t^n + \tau))$ is also a function of ℓ and we have

$$V(\Phi(t^n + \tau)) = V(\ell) = \zeta V_0 \quad (43)$$

from which the variable Lagrange multiplier ℓ at each time step can be obtained.

Equation (43) can be solved by several well-established nonlinear equation solvers. In the present study, the bi-sectioning algorithm is employed due to its robustness. The bi-sectioning algorithm is initialized by setting a lower bound ℓ_1 and an upper bound ℓ_2 for the Lagrange multiplier ℓ . In the present numerical study, it is initially chosen that $\ell_1 = 0$, which will cause a maximum volume increase since the normal velocity v_n in (37) will be maximized and thus the whole free boundary moves outwardly, and $\ell_2 = 10^5$, which may generate a significant volume decrease since almost all of the normal velocities become negative due to the relatively small strain energy density and thus almost the whole free boundary moves inwardly. The interval which bounds the Lagrange multiplier is halved and the Lagrange multiplier is given by $\ell = (\ell_1 + \ell_2)/2$, from which the normal velocities v_n in (37) as well as the extension velocities v_n^e , which will be discussed later, can be determined and thus the generalized

expansion coefficients α in (25) can be updated. The implicit level set function in Eq. (11) is also updated and the volume $V(\ell)$ can be finally obtained from Eq. (4). Based on the sign of the error in solving Eq. (43) using this volume, either the lower bound ℓ_1 or the upper bound ℓ_2 can be updated. The interval which bounds the Lagrange multiplier can be repeatedly halved until its size is less than the convergence criteria.

By using the present explicit volume constraint handling approach, convergence of the volume constraint function can be guaranteed during the iterations and there is no need for the initial designs to satisfy the volume constraint exactly. The complicated boundary integrations are avoided and the additional efforts to put the iteration back to the feasible set is unnecessary. Hence, the present explicit volume constraint handling approach would outperform those implicit volume constraint handling approaches in the literature [Osher and Santosa (2001); Wang, Wang, and Guo (2003); Wang and Wang (2006a)].

3.4 Simultaneous Shape and Topology Optimization

According to the present level set method, for the optimal design, we have $v_n|_{\Gamma_M} = 0$ at the free boundary. It can thus be obtained that

$$\boldsymbol{\varepsilon}^T \mathbf{C} \boldsymbol{\varepsilon}|_{\Gamma_M} = \ell \quad (44)$$

which implies that the strain energy density is constant everywhere along the optimal free boundary Γ_M since the Lagrange multiplier ℓ is spatial-independent. This is also the objective of the classical shape optimization methods based on a shape sensitivity analysis [Rozvany (1998); Sokolowski and Zolesio (1992)]. Hence, the present level set method can perform the free boundary-based topology optimization and shape optimization simultaneously. In most shape optimization applications, a Lagrangian formulation of boundary propagation was used to achieve the optimality condition and obtain an optimal shape of the structure [Rozvany (1998); Sokolowski and Zolesio (1992)]. The moving boundary is usually discretized with a set of design variables directly controlling the exterior and interior bound-

aries. Only an explicit boundary representation method was used and the boundary changes can be accomplished only if the connectivity of the boundaries does not change since there is a severe limitation that only a structure of a fixed topology can be optimized. In the present level set method, both shape and topology can be optimized simultaneously. The whole design domain is implicitly represented by a level set function $\Phi(\mathbf{x})$ and the moving free boundary is represented by the zero level sets. Significant topological changes can be easily handled and captured such as developing sharp corners, breaking apart, merging together or even disappearing. Hence, the present level set method can be more powerful than the classical shape optimization methods.

3.5 Extension Velocities

In the present study, a physically meaningful extension velocity method without the additional PDE solving procedure [Mallad, Sethian, and Vemuri (1996)] is presented. According to Eq. (37), a natural extension of the normal velocity v_n at the free boundary can be obtained if the strain field $\boldsymbol{\varepsilon}(\mathbf{u})$ is extended to the entire design domain D by assuming $\boldsymbol{\varepsilon}(\mathbf{u}) = 0, \mathbf{u} \in (D \setminus \Omega)$. Nevertheless, this extension will introduce an apparent discontinuity in the extension velocity field at the free boundary since the strain field is not continuous across the free boundary. To guarantee a smooth progress of the free boundary, this discontinuity should be eliminated. Hence, a linear smoothing filter is introduced in the narrowband region around the free boundary, which is defined as

$$\Xi = \left\{ \mathbf{x} \in \mathbb{R}^d \mid |d(\mathbf{x})| \leq \Delta \right\} \quad (45)$$

where Δ is the half bandwidth and $d(\mathbf{x})$ the distance to the interface $\Phi(\mathbf{x}) = 0$. The extension velocity v_n^e in the narrowband is smoothed as \widehat{v}_n^e by using a simple linear filter to achieve an excellent smoothing effect [Wang and Wang (2005a, 2006a)], which can be written as

$$\widehat{v}_n^e(\mathbf{x}) = k^{-1}(\mathbf{x}) \sum_{\mathbf{p} \in N(\mathbf{x})} w(\|\mathbf{p} - \mathbf{x}\|) v_n^e(\mathbf{x}) \quad (46)$$

where

$$w(\|\mathbf{p} - \mathbf{x}\|) = r_{\min} - \|\mathbf{p} - \mathbf{x}\| \quad (47)$$

$$k(\mathbf{x}) = \sum_{\mathbf{p} \in N(\mathbf{x})} w(\|\mathbf{p} - \mathbf{x}\|) \quad (48)$$

in which $N(\mathbf{x})$ is the neighborhood of $\mathbf{x} \in \Xi$ in the filter window and r_{\min} the window size. Hence, the overall extension velocity can be given as

$$v_n^e(\mathbf{x}) = \begin{cases} \boldsymbol{\varepsilon}^T \mathbf{C} \boldsymbol{\varepsilon} - \ell & \mathbf{x} \in \mathbb{R}^d \mid d(\mathbf{x}) < -\Delta \\ \widehat{v}_n^e(\mathbf{x}) & \mathbf{x} \in \Xi \\ -\ell & \mathbf{x} \in \mathbb{R}^d \mid d(\mathbf{x}) > \Delta \end{cases} \quad (49)$$

Using this extension velocity field $v_n^e(\mathbf{x})$, smooth time advance of the moving free boundary can be obtained due to the smoothing effect of the velocity filtering operation. Furthermore, the present velocity filtering is also able to regularize the well-known ill-posed shape and topology optimization problem [Bendsøe and Sigmund (2003); Wang and Wang (2005a)] into a well-posed one, similar to the popular sensitivity filtering approach in the SIMP method [Bendsøe and Sigmund (2003)].

3.6 Nucleation of New Holes

From the Hamilton-Jacobi PDE (5), the level set function can be approximately updated as

$$\Phi(t^{n+1}) = \Phi(t^n) - \tau v_n^e |\nabla \Phi| \quad (50)$$

Hence, inside the material domain, $\Phi(t^n) < 0$, in a region with negative extension velocities, $v_n^e < 0$, a new hole will be created at the position where the following condition can be satisfied:

$$\tau v_n^e |\nabla \Phi| < \Phi(t^n). \quad (51)$$

In the present level set method, the timestep size τ can be relatively large since the use of large timesteps is permitted, but it cannot be too large due to the accuracy requirement. According to Eq. (37), the negative velocity v_n^e is also with a limitation as $-\ell \leq v_n^e < 0$ and the minimum value is obtained when the material is least effectively used such that $\boldsymbol{\varepsilon}^T \mathbf{C} \boldsymbol{\varepsilon} = 0$. Hence, the magnitude of the norm of the spatial gradient $|\nabla \Phi|$ can play a most significant role in nucleation of new holes. In the present level set method, due to the elimination of reinitialization, a relatively steep level set

function may be developed even if the level set function is initialized as a signed distance function $|\nabla\Phi| = 1$. According to Eq. (50), the spatial gradient of the updated Φ is closely related with the spatial gradient of the extension velocity v_n^e , which is determined by the spatial gradient of the strain energy density, according to Eq. (49). Hence, inside a region with negative velocities, creation of a new hole at a site may happen when the strain energy density is quite small but its spatial gradient is large enough. More generally, the site to create a new hole should satisfy the following condition:

$$\begin{aligned} \min \quad & (\boldsymbol{\varepsilon}^T \mathbf{C} \boldsymbol{\varepsilon} - \ell) |\nabla(\boldsymbol{\varepsilon}^T \mathbf{C} \boldsymbol{\varepsilon})| \\ \text{s.t.} \quad & \Phi < 0 \end{aligned} \quad (52)$$

Hence, this nucleation mechanism is physically meaningful.

The present idea of nucleation of new holes can be similar to that of the popular element removal techniques such as the evolutionary structural optimization (ESO) approach [Xie and Steven (1993)] for topology optimization, in which the material in a design domain which is not structurally active is considered as inefficiently used and can thus be slowly removed. However, the ESO approach is only an intuitive method without a proof of optimality [Rozvany (2001b,a); Zhou and Rozvany (2001); Wang and Wang (2005a)] and the spatial gradient of the strain energy density is not considered in its deletion criteria. Hence, the present condition as shown in Eq. (52) can be more complete for nucleation of new holes. Furthermore, prescribed deletion criteria are not needed and new holes are created in an automatic manner during the level set evolution. In the final optimum, further nucleation of new holes is impossible and thus in the material domain we have $v_n^e \geq 0$, or $\boldsymbol{\varepsilon}^T \mathbf{C} \boldsymbol{\varepsilon} \geq \ell$.

The present level set method may create new holes during the level set evolution, similar to the ESO approach [Xie and Steven (1993)], the bubble method [Eschenauer, Kobelev, and Schumacher (1994)], or the topological gradient method [Burger, Hackl, and Ring (2004)]. Since the final design may have more holes than the initial design, the present method is less sensitive to

the initialization and the probability of converging to a local minimum can be greatly reduced. This can be a significant improvement over the standard level set methods, which only allow limited topological changes [Burger (2004)].

4 Examples and Discussion

Numerical examples in two dimensions are provided to illustrate the accuracy and efficiency of the present BIBO time-stable meshfree level set method for structural shape and topology optimization. Unless stated otherwise, all the units are consistent and the following parameters are assumed as: the Young's elasticity modulus $E = 1$ for solid materials, and Poisson's ratio $\nu = 0.3$. Furthermore, $\Delta = 1$ grid size for the half bandwidth size, $r_{\min} = 2.4$ grid size for the filter window size. For all examples, a fixed rectilinear mesh is specified over the entire design domain D as a global mesh. The present algorithm is terminated when the relative difference between two successive objective function values is less than 10^{-5} or when the given maximum number of iterations has been reached. The topologies are given in black-and-white form based on the scalar value of the implicit function $\Phi(\mathbf{x})$, as defined in Eq. (1).

4.1 A Michell Type Structure

The present meshfree level set method is applied to the classical Michell type structure problem, as shown in Fig. 3(a), in which a theoretical Michell's solution is available [Michell (1904)], as shown in Fig. 3(b). The whole design domain D is a rectangle of size $L \times H$, the two bottom corners have the pinned supports, and a unit vertical point force P is applied at the middle point of the bottom side. As shown in Fig. 3(b), the theoretical optimum topology consists of two 45° arms extending from the supports towards an approximately 90° central fan section which extends upwards from the point of application of the force [Wang and Tai (2005)]. In the present study, it is assumed that $L = 2$, $H = 1.2$, $P = 1$, and a pre-specified material volume fraction $\zeta = 0.3$. The domain D is discretized with a fixed rectangular mesh of 100×60 as the global mesh for the

present S-FEM model. Due to the symmetry, only a half structure is used in the physical analysis.

The design with holes shown in Fig. 4(a) is taken as the initial design and a timestep size of $\tau = 1.0$ together with a free shape parameter of $c = 0.01$ is adopted to perform the simultaneous shape and topology optimization using the present level set method. Figure 4 displays the evolution history of the final design. It can be seen that drastic topological changes in a single time step have been obtained due to the use of a relatively large timestep size such that the geometric deformation at the moving free boundary can be relatively large. This is a big difference between the present BIBO time-stable level set method, which permits the use of large timesteps, and the standard CFL-constrained level set methods [Sethian (1999); Osher and Fedkiw (2002); Wang, Wang, and Guo (2003); Allaire, Jouve, and Toader (2004)], in which the motion of the free boundary is limited by the grid size in a single timestep to satisfy the CFL condition. The final topology consisting of two arms and a central fan section is quite similar to the theoretical optimum topology for a truss-like structure as shown in Fig. 3(b) and thus the accuracy of the present meshfree level set method can be verified. The convergence of the objective and volume functions is shown in Fig. 5. It can be seen that rapid convergence in both the objective and volume functions has been obtained due to the use of a large timestep and the present volume constraint handling approach. The increase of the objective function at the first timestep is due to the significant decrease of the structural volume to satisfy the volume constraint. The subsequent stable decrease of the objective function can justify the significant topological changes, as shown in Fig. 4. Although the volume constraint is not satisfied exactly at the initial time, the volume function converges in a single timestep for this problem and it can be guaranteed that the subsequent designs be feasible during the level set evolution. This is a significant advantage over the implicit volume constraint handling approaches [Wang, Wang, and Guo (2003); Wang and Wang (2006a)], in which apparent fluctuation of the structural volume exists in the whole evolution procedure and

the final design may thus be infeasible. The convergence of the final design shown in Fig. 4(h) can be further indicated by the good agreement between material volume in the S-FEM physical model and the non-negative scalar extension velocity field, as shown in Fig. 6. Theoretically, the zero scalar velocity curve should correspond to the free boundary of the optimal design exactly such that further movement and geometric deformation along the decent direction of the free boundary are actually prevented.

Furthermore, this problem is investigated again by using an initial design without a hole. The design without any holes shown in Fig. 7(a) is taken as another initial guess and a timestep size of $\tau = 0.001$ together with a free shape parameter of $c = 0.0001$ is adopted. Figure 7 displays the evolution history of the final design using the present meshfree level set method. It can be seen that drastic topological changes mainly due to the creation of new holes have been obtained. The nucleation capacity of the present method without using the classical topological derivatives [Sokolowski and Żochowski (2001)] is thus demonstrated. In the literature [Burger, Hackl, and Ring (2004); Allaire, de Gournay, Jouve, and Toader (2005); Amstutz and Andrä (2006)], topological derivatives are usually incorporated into the shape derivatives-based level set methods to achieve the nucleation capacity, but the Hamilton-Jacobi equation may be modified and the level set evolution may become more complicated. As aforementioned, the present nucleation mechanism is physically meaningful and there is no need to modify the Hamilton-Jacobi equation. Comparing Fig. 7 with Fig. 4, it can be obtained that the final design can be less sensitive to the initial guesses due to the capacity of the present method for nucleation of new holes. In the standard level set methods, nucleation of new holes is not allowed for and therefore the final design is largely dependent of the initial designs [Allaire, Jouve, and Toader (2004)]. The final topology shown in Fig. 7(h) is similar to the theoretical optimum topology as shown in Fig. 3(b) and thus the accuracy of the present method can again be verified. The convergence of the objec-

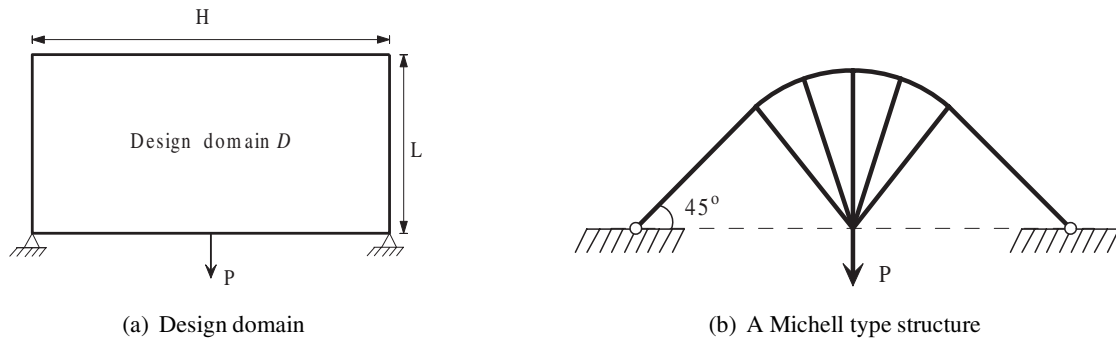


Figure 3: Optimal design problem for a Michell type structure with fixed supports.

tive and volume functions is shown in Fig. 8. It can be seen that rapid and stable convergence in both the objective and volume functions has been achieved due to the present BIBO time stability. The stable decrease in the objective function can justify the present significant topological changes, such as creation of new holes and splitting of connected components, as shown in Fig. 7. For this case, the volume constraint can be satisfied accurately after a single timestep to keep the designs feasible during the level set evolution due to the use of the present explicit volume constraint handling approach. Again, the convergence of the final design can be further indicated by the good agreement between the free boundary in the S-FEM physical model and the zero extension velocity curve, as shown in Fig. 9, as theoretically predicted.

4.2 A Short Cantilever Beam

The minimum compliance design problem of a short cantilever beam is shown in Fig. 10. The whole design domain D is a rectangle of size 2×1 with a fixed boundary ∂D (zero displacement boundary condition) on the left side and a unit vertical point load $P = 1$ applied at a fixed non-homogeneous Neumann boundary ∂D_N , the middle point of the right side. The prespecified volume fraction is $\zeta = 0.5$. A 80×40 mesh is used as the global mesh for the present S-FEM model. The distribution of the fixed RBF knots for the present level set method is uniform, as shown in Fig. 10 for illustrative purposes only.

For the initial design with holes as shown in

Fig. 11(a), the present level set method with a shape parameter $c = 0.001$ and a timestep size $\tau = 0.001$ is used to perform simultaneous shape and topology optimization. The evolution history of the final design is displayed in Fig. 11. It can be seen that rapid convergence in both shape and topology has been achieved due to the use of a relatively large timestep size while drastic topological changes are experienced during the evolution, such as splitting and merging connected components, creation of new holes and disappearance of structurally disconnected components. Hence, the advantage of the present BIBO time-stable level set method is again illustrated. Figure 12 displays the convergence of the objective and volume functions. It can be seen that the present level set method converges rapidly in terms of the total number of timesteps since its BIBO time stability permits the use of relatively large timesteps. This is a significant advantage of the present method over the standard finite difference-based level set methods for shape and topology optimization [Wang, Wang, and Guo (2003); Allaire, Jouve, and Toader (2004)], which converge slowly due to the strict CFL condition for the timestep size. Again, it can be seen that the structural volume can be almost conservative and the volume constraint can be accurately satisfied during the level set evolution due to the present explicit volume constraint handling approach. Figure 13 shows a comparison between the physical model and the non-negative scalar velocity field during the level set evolution. It can be seen that a good agreement between the

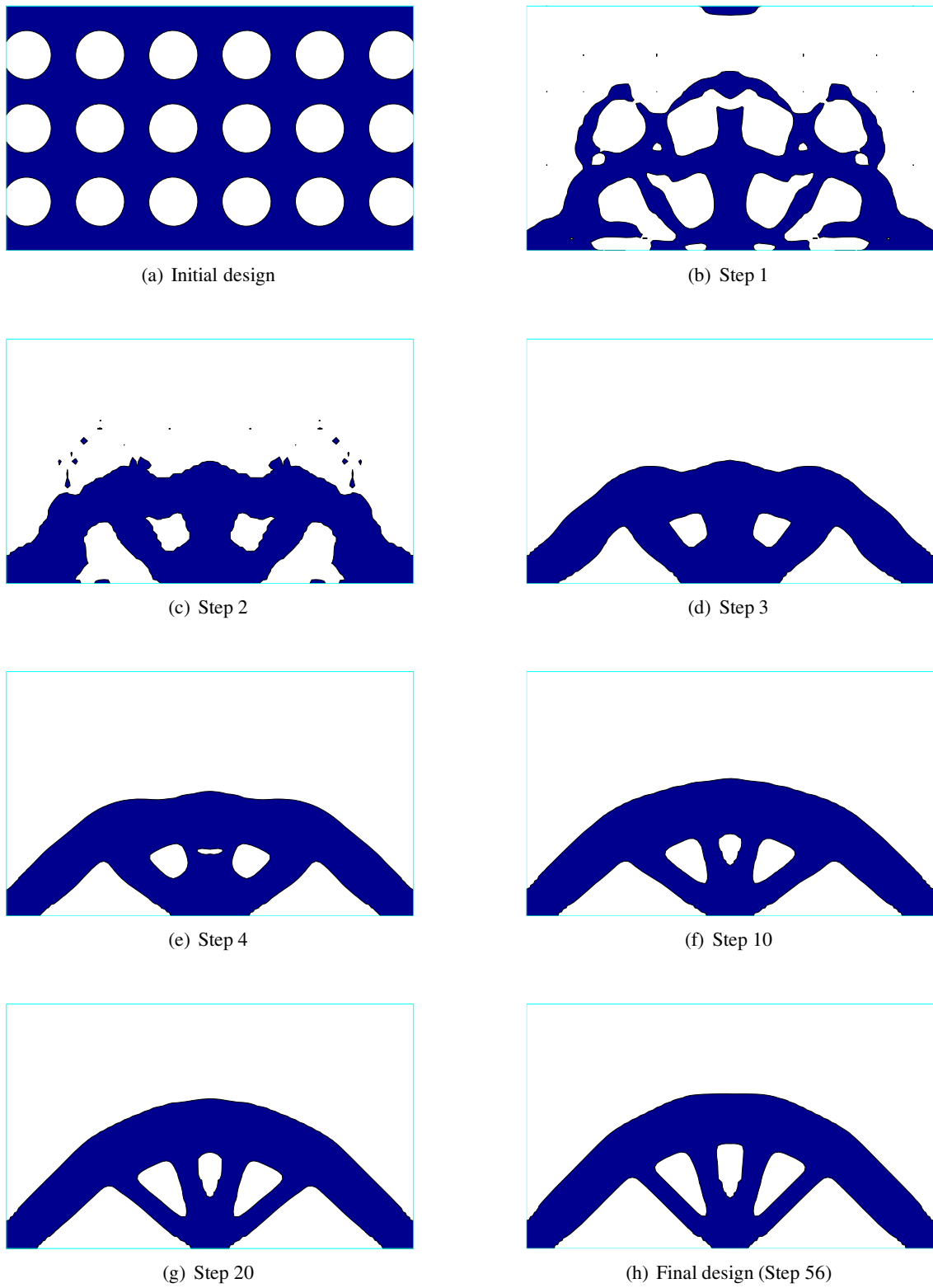


Figure 4: Evolution of the optimal design for the Michell type structure starting with an initial design with holes using the present level set method.

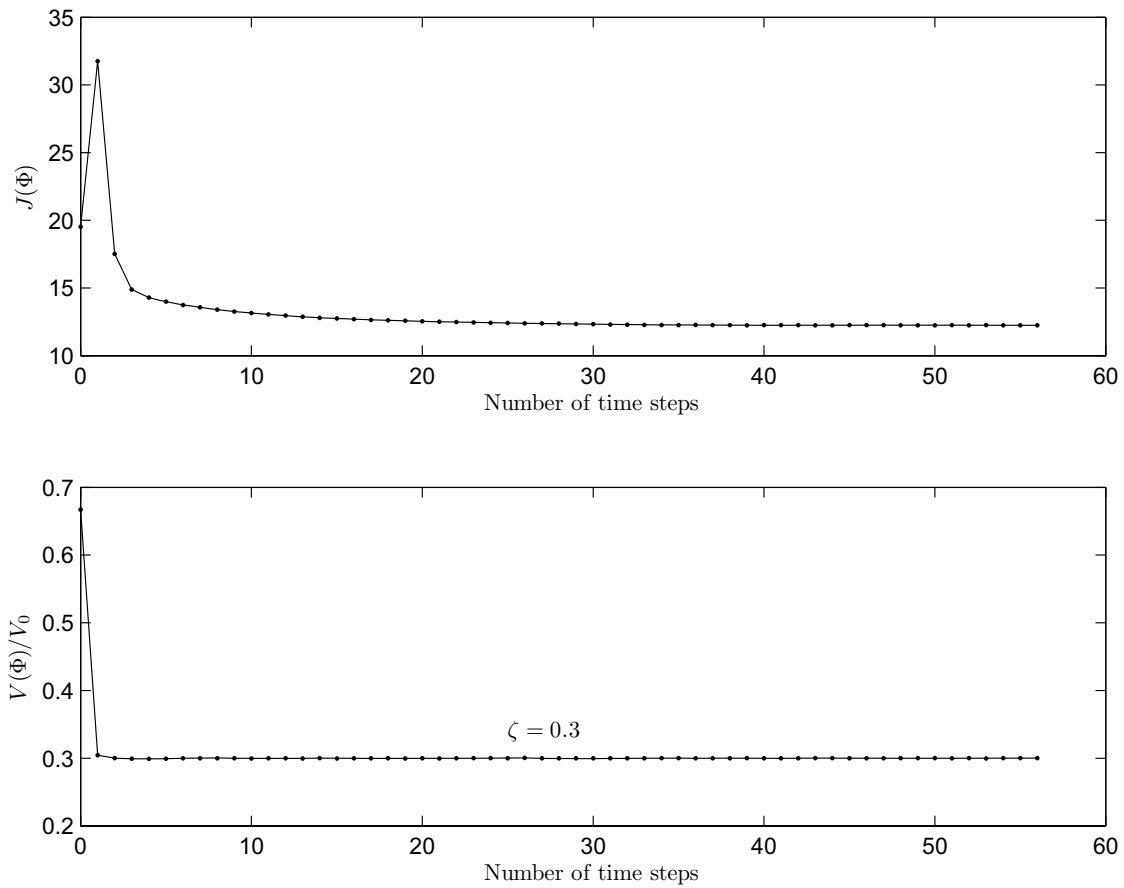


Figure 5: Convergence of the objective and volume functions for the Michell type structure starting with an initial design with holes using the present level set method.

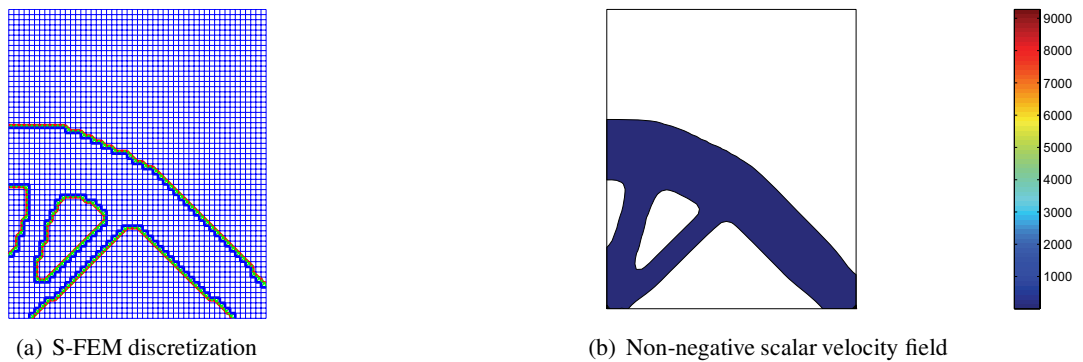


Figure 6: The final design for the Michell type structure starting with an initial design with holes using the present level set method.

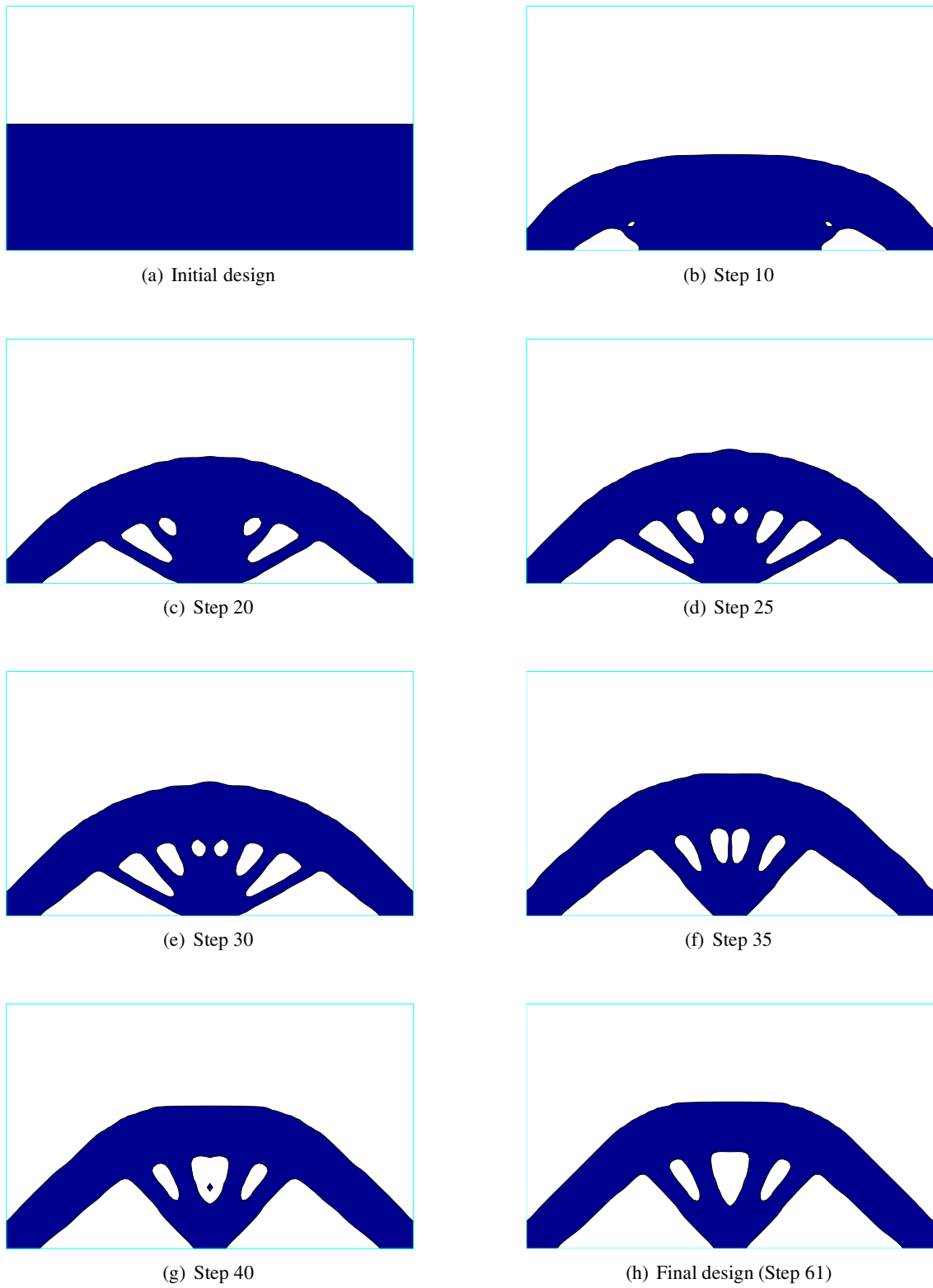


Figure 7: Evolution of the optimal design for the Michell type structure starting with an initial design without a hole using the present level set method.

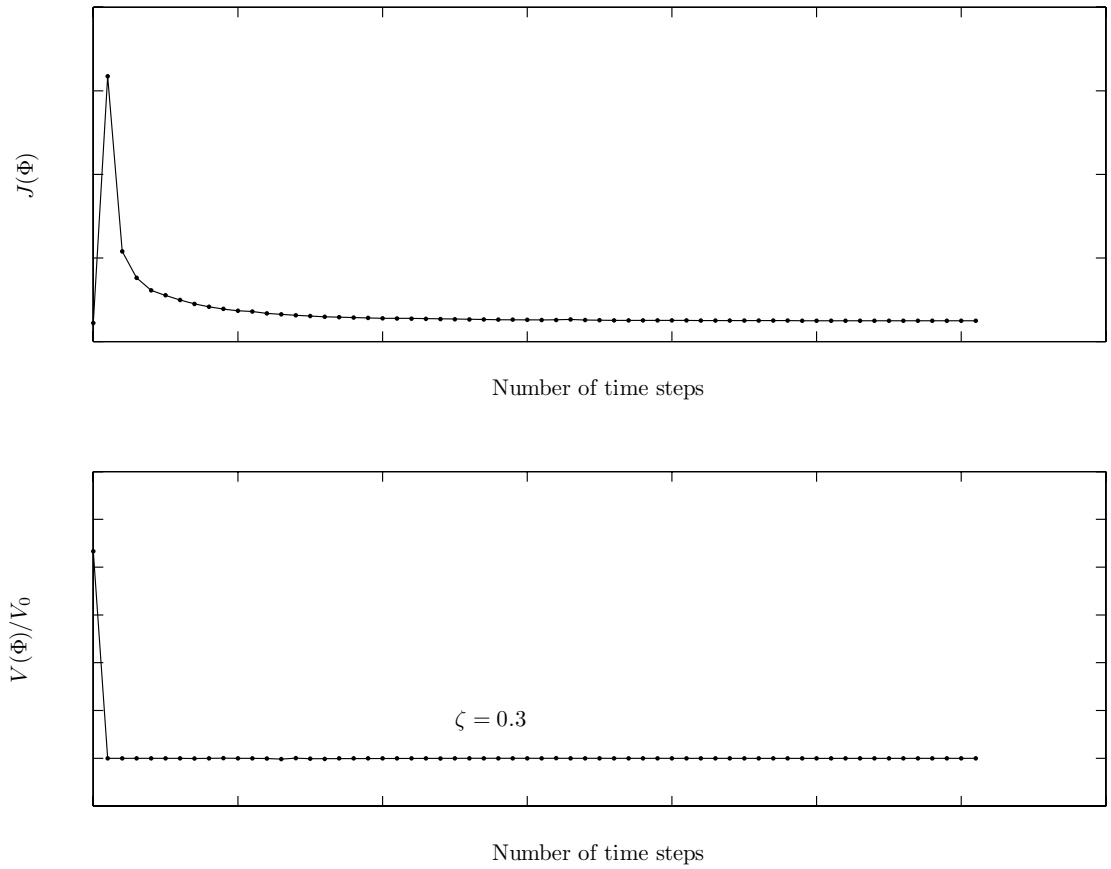


Figure 8: Convergence of the objective and volume functions for the Michell type structure starting with an initial design without a hole using the present level set method.

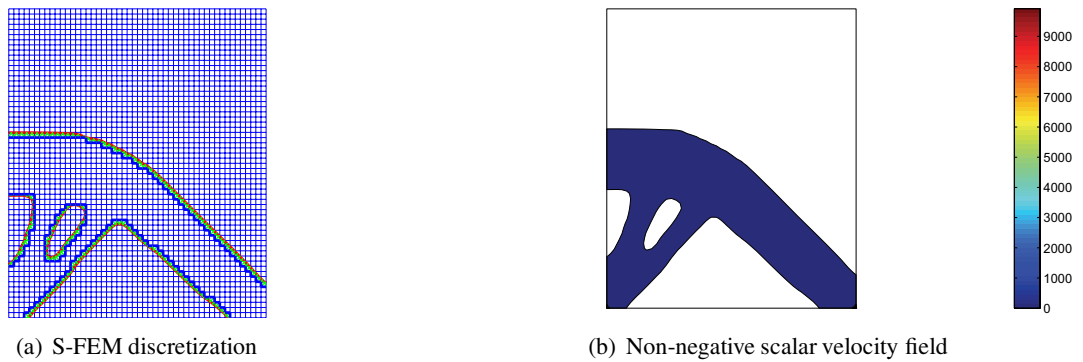


Figure 9: The final design for the Michell type structure starting with an initial design without a hole using the present level set method.

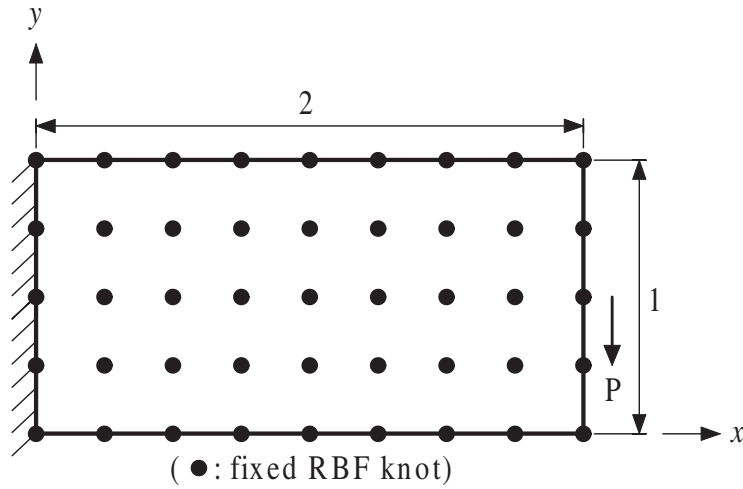


Figure 10: Minimum compliance design problem of a cantilever beam with a uniform RBF knot distribution.

Table 1: Effect of the free shape parameter c on the optimal solution.

Timestep τ	Shape parameter c	$J_{\min}(\Phi)$	Total number of timesteps
0.0001	0.0001	131.6439	100
	0.001	64.1511	100
	0.01	58.6389	61
	0.05	58.9288	28
0.001	0.0001	59.8658	100
	0.001	58.3471	24
	0.01	58.6310	100
0.01	0.00001	58.9704	100
	0.0001	58.5089	43
	0.001	58.5265	100
	0.01	59.9086	100

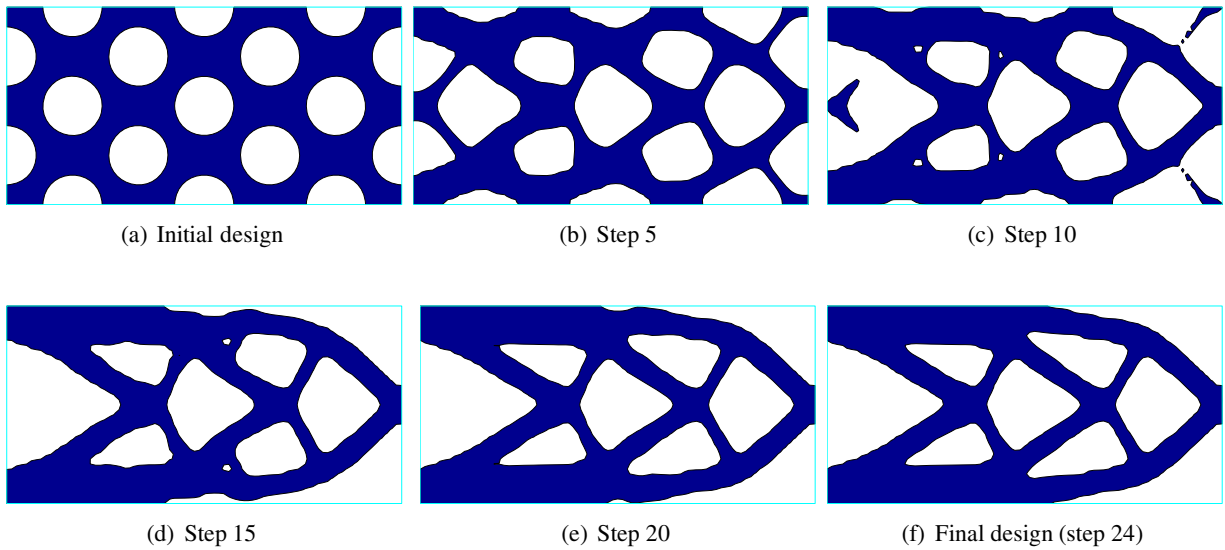


Figure 11: Evolution of the optimal design for the cantilever starting with an initial design with holes using the present level set method.

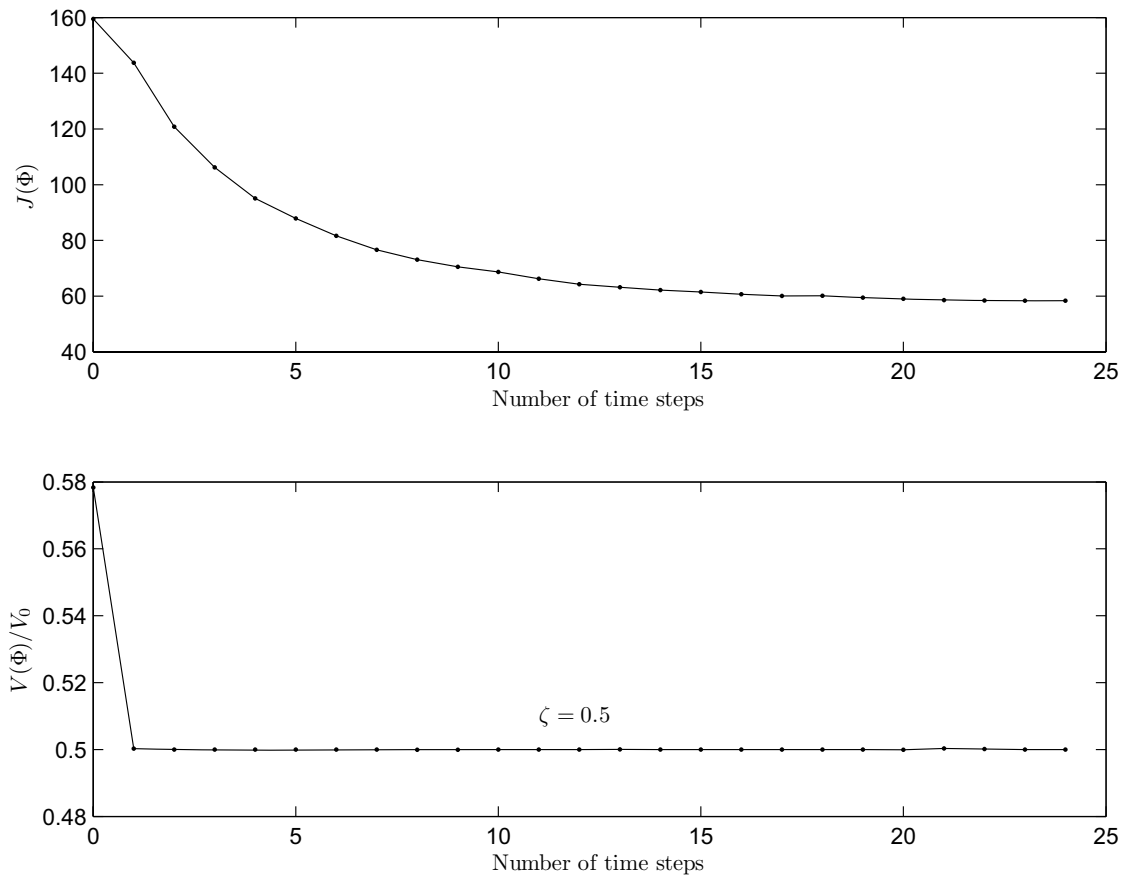


Figure 12: Convergence of the objective and volume functions for the cantilever starting with an initial design with holes using the present level set method.

physical model and the non-negative scalar velocity field can be finally arrived at, as theoretically predicted, though initially the difference between them is quite obvious. It should be noted that the physical model is consistent with the geometrical model due to the present S-FEM discretization and thus a high level of accuracy in estimating the velocity field as well as the strain energy density field can be expected. The evolution history of the strain energy density field is shown in Fig. 14. During the present level set evolution, the apparent heterogeneous strain energy density distribution in the initial design can be rapidly changed into an almost homogeneous distribution due to the present simultaneous shape and topology optimization, which agrees well with the theoretical prediction. The remaining small regions with large density values are due to the significant stress concentration at the loading or fixed boundary regions because of the local effects of the applied force, according to Saint-Venant's principal [Choi and Horgan (1977)], which cannot be eliminated totally and does not affect the objective function much due to the small sizes of those regions. Based on a trial and error procedure, the effect of the free shape parameter c on the optimal solution is listed in Table 1. It can be seen that for different timestep sizes, better solutions can be obtained when the parameter c gets larger until it reaches an optimal point. The convergence speed may become slow if both the shape parameter c and the timestep size τ are quite small. This observation can be consistent with those made in [Kansa, Powerb, Fasshauerc, and Ling (2004)] based on approximate solutions of PDEs using IMQ RBFs. This feature of RBF discretization can be attractive in the present shape and topology optimization since a broader search space can be explored without changing other settings and the probability of finding a solution closer to the global optimum is increased.

For the purpose of comparison, a standard level set method [Osher and Fedkiw (2002); Mitchell (2004)] coupled with an Ersatz material approach [Allaire (2001); Allaire, Jouve, and Toader (2004)] in the physical model together the present explicit volume constraint handling approach is

also developed to solve this minimum compliance design problem. In this level set method, a second-order ENO (essentially non-oscillatory) upwind scheme is used for the propagation of the free boundary and a third-order reinitialization algorithm is adopted to minimize the numerical diffusion around the location of the original interface [Tsai and Osher (2003)], and an aggressive CFL number of 0.9 is used to drive a fast convergence. Reinitialization as an auxiliary step is performed every 5 times of transport and the maximum number of timesteps is specified as 1000.

For the same initial design with holes as shown in Fig. 11(a), the evolution history of the final design using the standard level set method is displayed in Fig. 15. It can be seen that topology optimization is performed by splitting connected components. The topological changes are rather smooth and the final design has fewer holes than the initial design. The final design shown in Fig. 15(f) can be quite similar to the one shown in Fig. 11(f) using the present level set method. However, the convergence speed is quite slow due to the CFL condition for time stability, comparing the convergence history shown in Fig. 16 with the one using the present BIBO time-stable level set method as shown in Fig. 12. Due to the decrease of the volume to drive the design to the feasible set, the objective function value may increase rather than decrease in the first few timesteps. The volume constraint can be almost exactly satisfied after the first few timesteps because of the present volume constraint handling approach. As a comparison, the implicit volume constraint handling approaches in [Wang, Wang, and Guo (2003); Wang and Wang (2006a)] cannot satisfy the volume constraint accurately and significant fluctuation of the total volume may be observed in [Wang, Wang, and Guo (2003); Wang and Wang (2006a)]. Furthermore, it should be noted that the geometrical changes are quite slow due to the CFL condition and some structurally disconnected components cannot be eliminated completely when the present convergence criteria have been reached, as shown in Fig. 15(f). Theoretically, the structurally disconnected components can be completely eliminated by the level set evolution due to their neg-

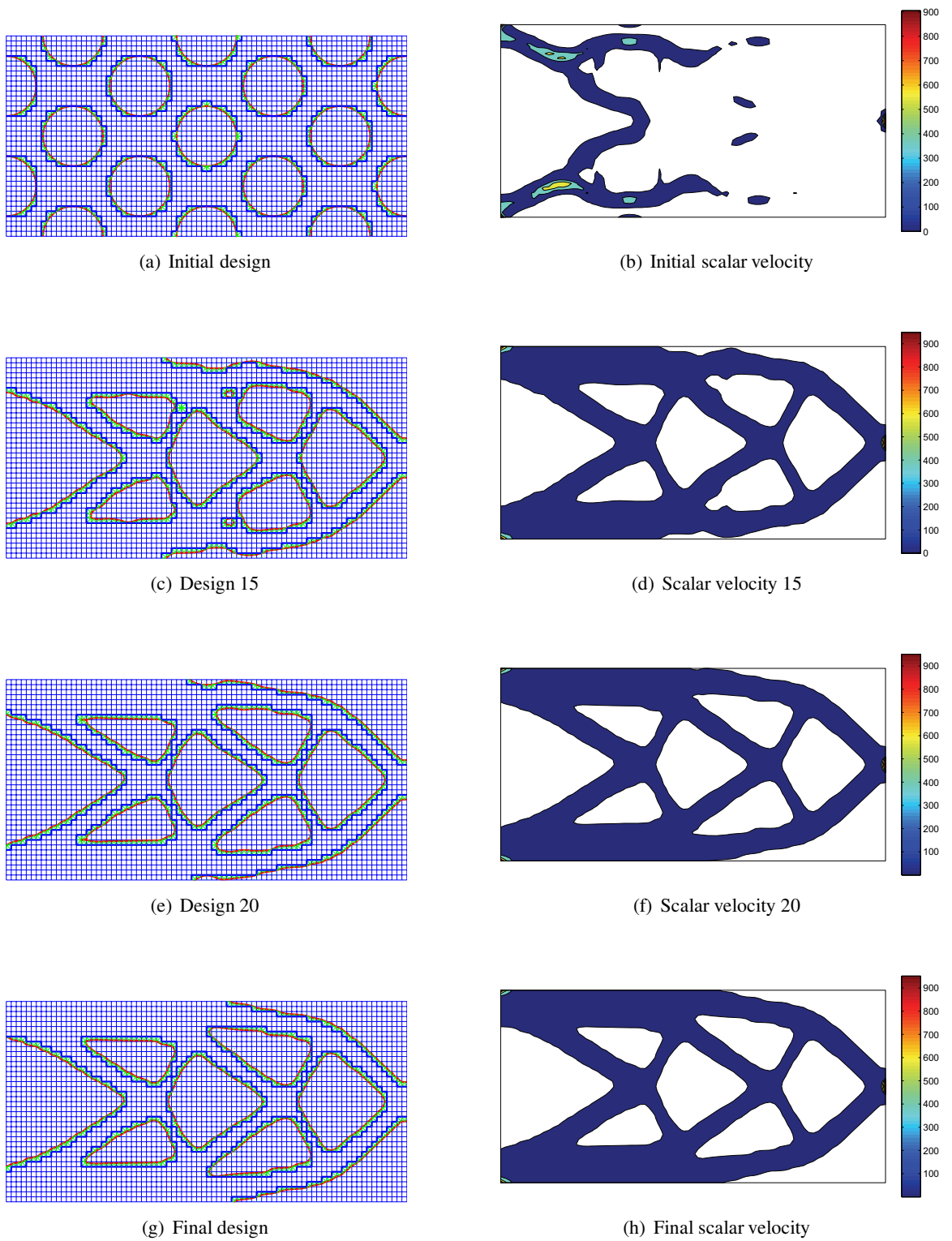


Figure 13: Comparison between the physical model and the non-negative scalar velocity field ($v_n^e \geq 0$) for the cantilever starting with an initial design with holes using the present level set method.

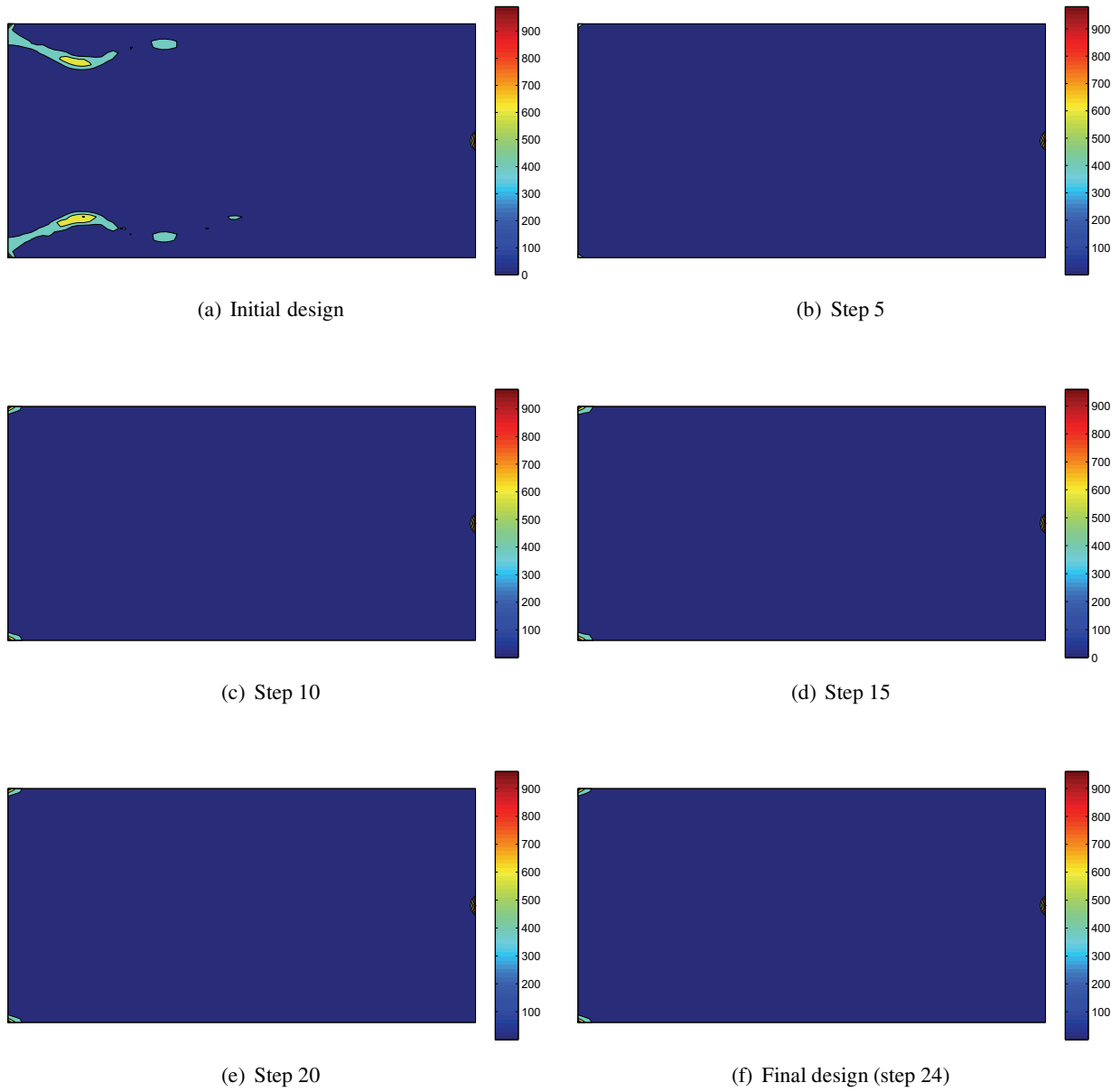


Figure 14: Evolution of the strain energy density field of the optimal design for the cantilever starting with an initial design with holes using the present level set method.

ative velocities ($\boldsymbol{\varepsilon}^T \mathbf{C} \boldsymbol{\varepsilon} = 0$). As shown in Fig. 17, the final design shown in Fig. 17(a) cannot reach a good agreement with the non-negative scalar extension velocities shown in Fig. 17(b). Hence, more iterations are needed to eliminate those disconnected components and to reach a better agreement between the geometry and the normal velocities and thus the computational cost may become much higher. Figures 17(c) and 17(d) show that the disconnected components can be eliminated and a better agreement between the geometry and the scalar velocity field can be achieved when 1000 designs are produced. Since the Ersatz material approach is used in the standard level set method, the physical model cannot be consistent with the geometrical model and a relatively low level of accuracy in evaluating the objective function and the strain field can be expected, compared with the present consistent S-FEM model, in which a more accurate modeling of the free boundary is provided, as shown in Fig. 18.

The capacity of the present level set method for nucleation of new holes is to be further discussed. A design with a single hole as shown in Fig. 19(a) is chosen as the initial design to perform the simultaneous shape and topology optimization again. Since the volume of the initial design with a volume fraction of 0.9649 is far higher than the the desired volume, in a single time step, the Lagrange multiplier will become too large and the resulting negative extension velocities are too high such that the structural connectivity may be broken due to the use of a large timestep. In this study, the approach proposed by the authors in [Wang and Wang (2006a)] is adopted, in which a fixed Lagrange multiplier was used to decrease the material volume in a stable manner. For this example, we set the fixed Lagrange multiplier as $\ell = 20$, the shape parameter $c = 0.001$ and the timestep size $\tau = 0.001$. Figure 19 displays the evolution history of the final design using the present level set method. It can be seen that creation of new holes is obtained and the final design has more holes than the initial design due to the present physically meaningful nucleation mechanism. The final design shown in Fig.

19(f) can even be similar to the one shown in Fig. 11(f) under this setting. Hence, the present level set method can be less sensitive to the initial designs due to its nucleation capacity. The convergence of both the objective and constraint functions is shown in Fig. 20. It can be seen that an uphill climbing process in the objective function is involved due to the dominant volume decrease to achieve a feasible design. Compared with the convergence history shown in Fig. 12 using an initial design with more holes, this convergence needs more iterations since more efforts are needed to drive the volume to the feasible set.

The design with a single hole as shown in Fig. 19(a) is further investigated using the standard level set method and Fig. 21 displays the evolution history of the final design. It can be seen that creation of new holes is not permitted and the final design cannot have more holes than the initial design due to the lack of a nucleation mechanism in the standard level set methods [Sethian (1999); Osher and Fedkiw (2002); Wang, Wang, and Guo (2003); Allaire, de Gournay, Jouve, and Toader (2005)]. Hence, the final design converges to a local optimum and may become largely dependent of the initial designs. The convergence history of both the objective and constraint functions is shown in Fig. 22. It can be seen that the uphill climbing process in the objective function needs significantly much more timesteps due to the strict CFL condition. The volume constraint can be almost exactly satisfied after the volume has been driven to the feasible set due to the use of the present volume constraint handling approach.

The capacity of the present consistent meshfree level set method for nucleation of new holes is further demonstrated by using an initial design without any holes. A design without a hole and with a volume fraction as prescribed ($\zeta = 0.5$) as shown in Fig. 23(a) is chosen as the initial design. Figure 23 shows the evolution history of the final design using the present level set method. It can be seen that creation of new holes is allowed for and the final design have three holes, though the initial design does not have a hole. Hence, the final design is less sensitive to the initial design due to the present nucleation capacity. This final

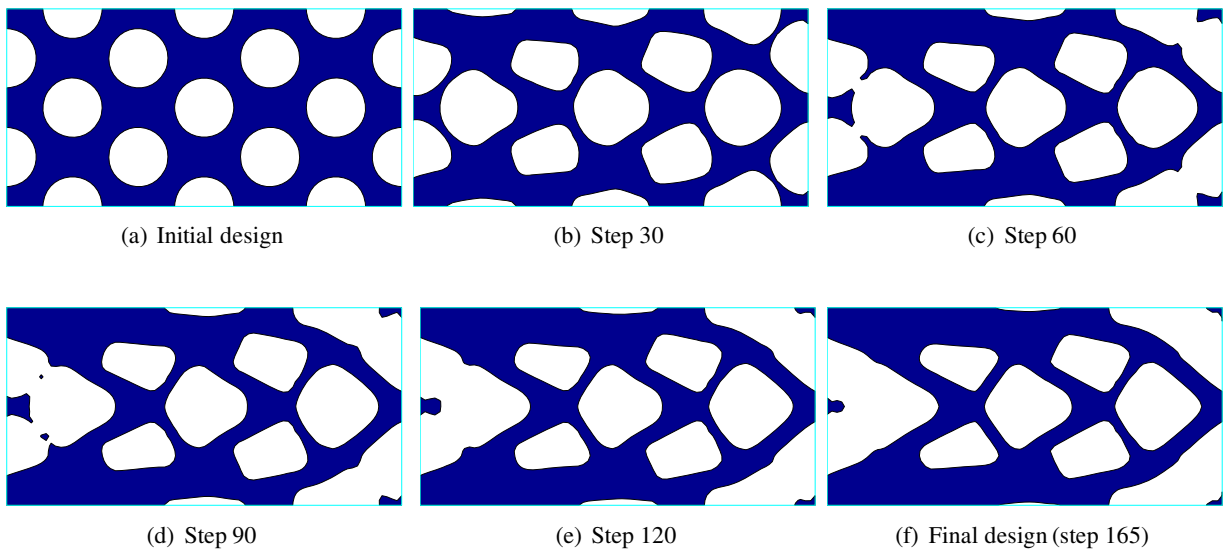


Figure 15: Evolution of the optimal design for the cantilever starting with an initial design with holes using a standard level set method.

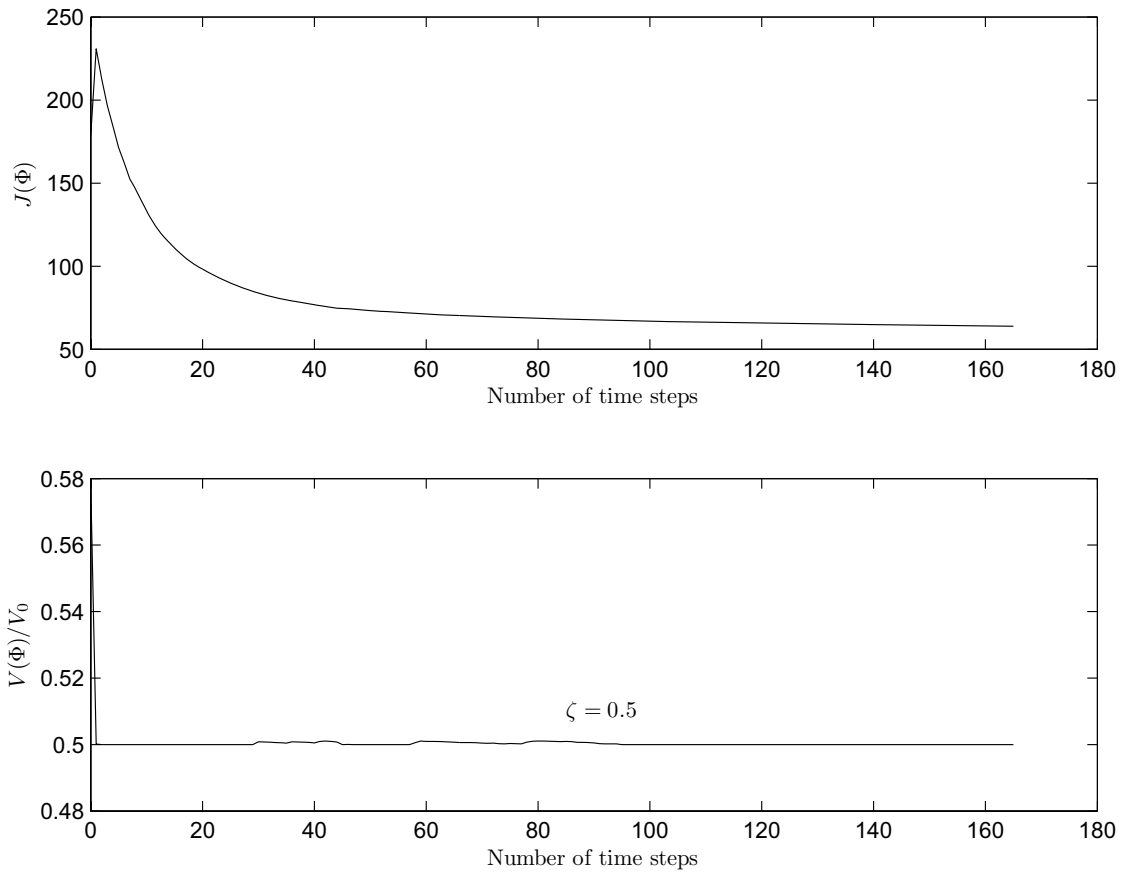


Figure 16: Convergence of the objective and volume functions for the cantilever starting with an initial design with holes using a standard level set method.

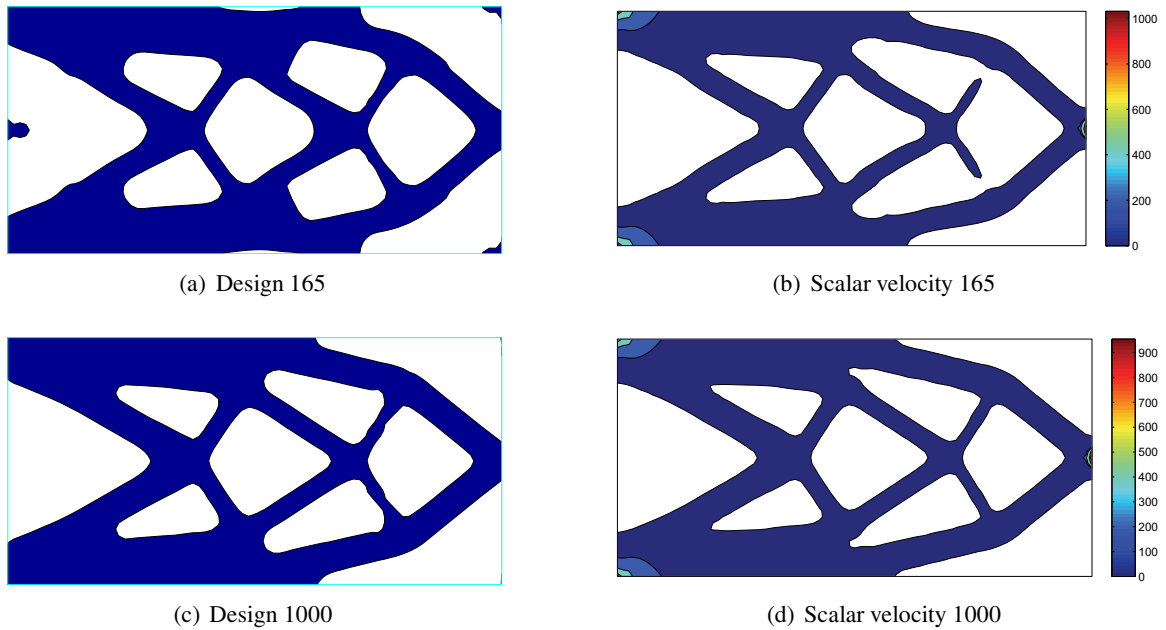


Figure 17: Comparison between the geometry and the scalar velocity ($v_n^e \geq 0$) for the cantilever starting with an initial design with holes using a standard level set method.

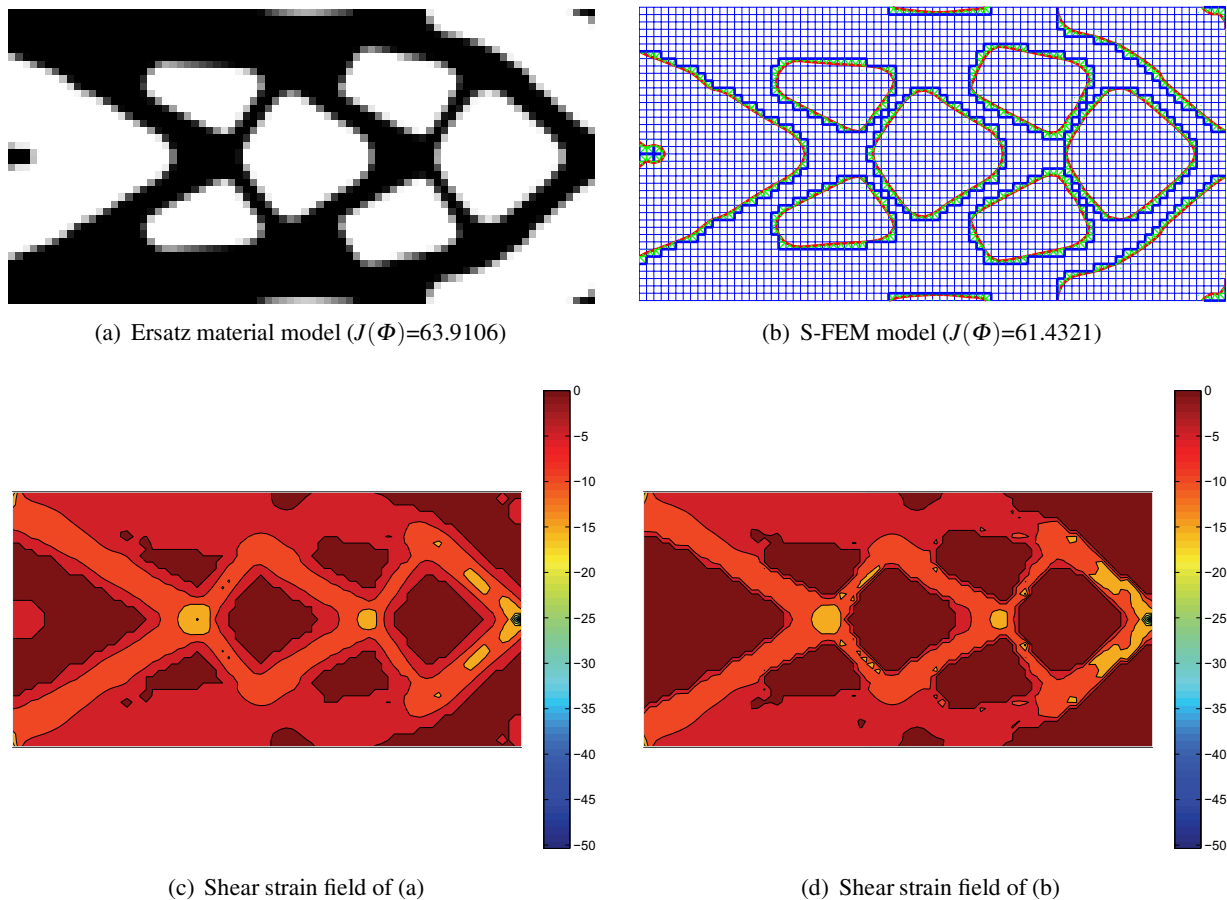


Figure 18: Comparison of the physical models for the design 165.

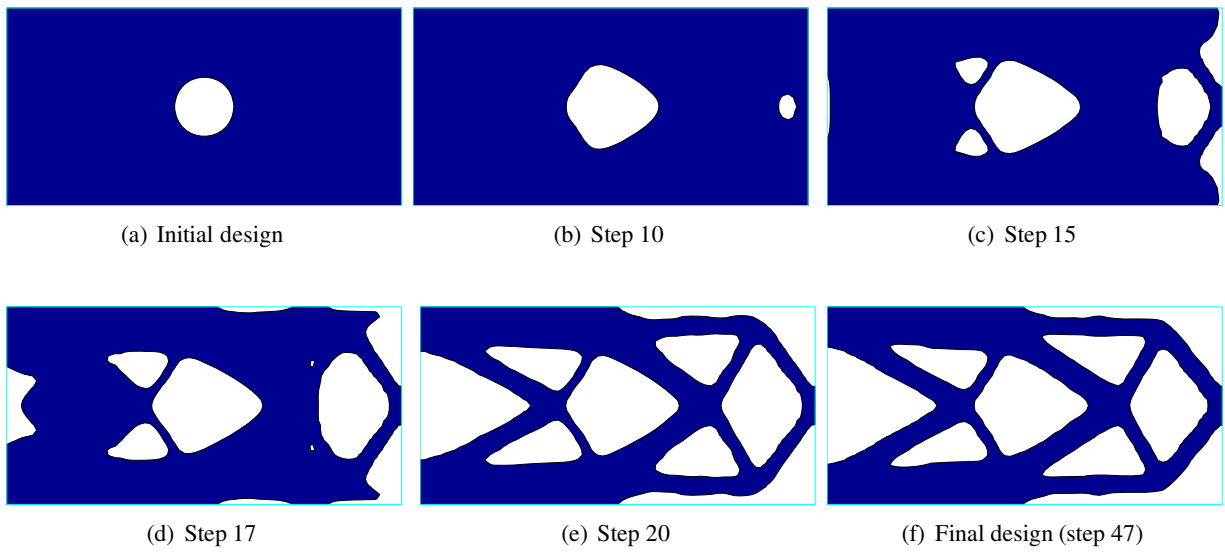


Figure 19: Evolution of the optimal design for the cantilever starting with an initial design with a single hole using the present level set method.

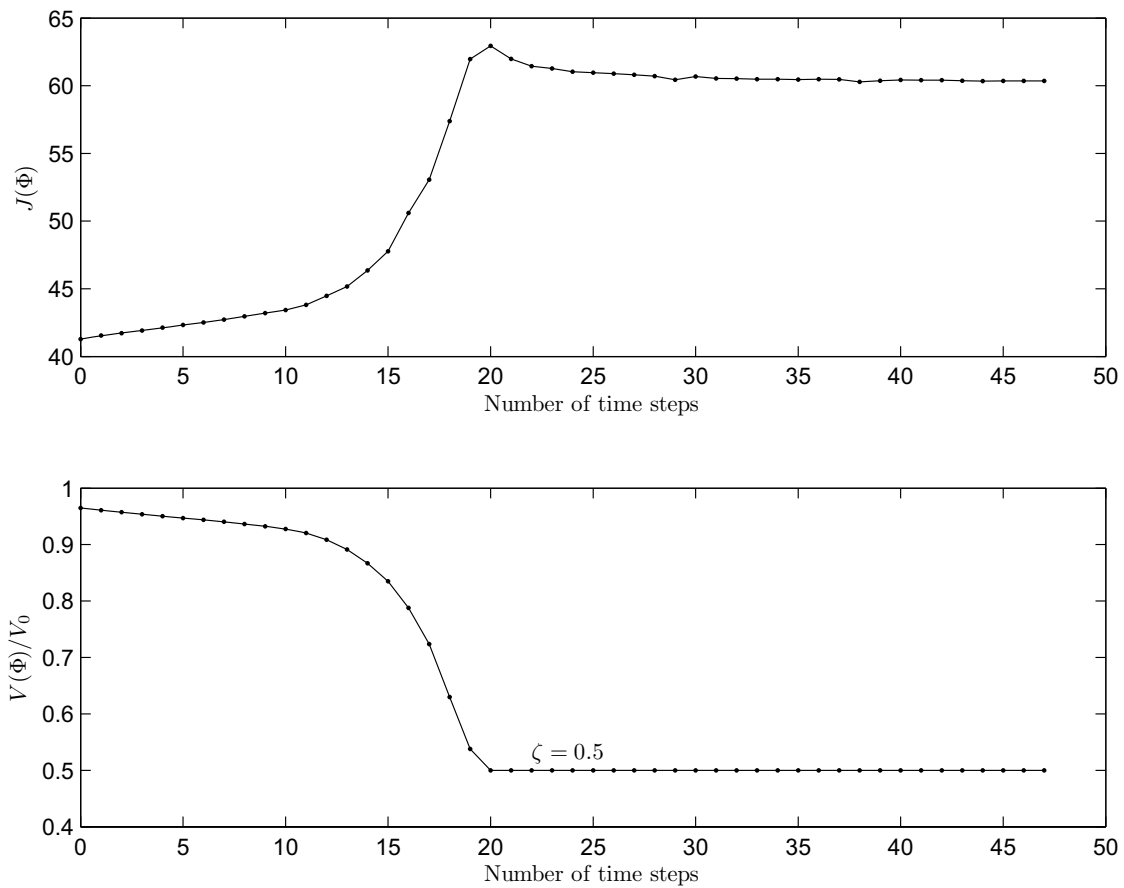


Figure 20: Convergence of the objective and volume functions for the cantilever starting with an initial design with a single hole using the present level set method.

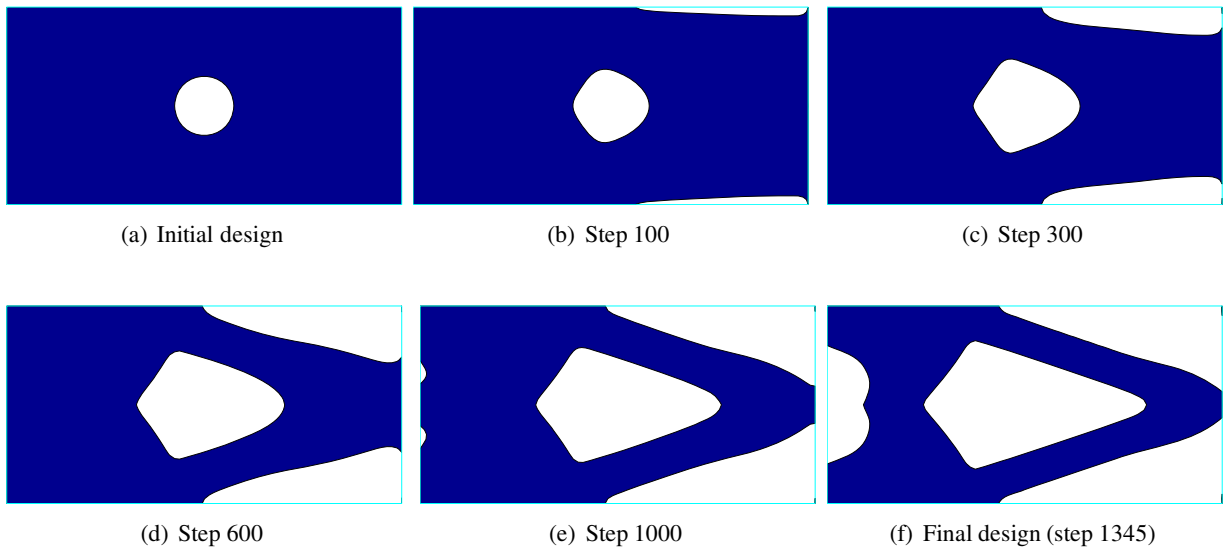


Figure 21: Evolution of the optimal design for the cantilever starting with an initial design with a single hole using a standard level set method.

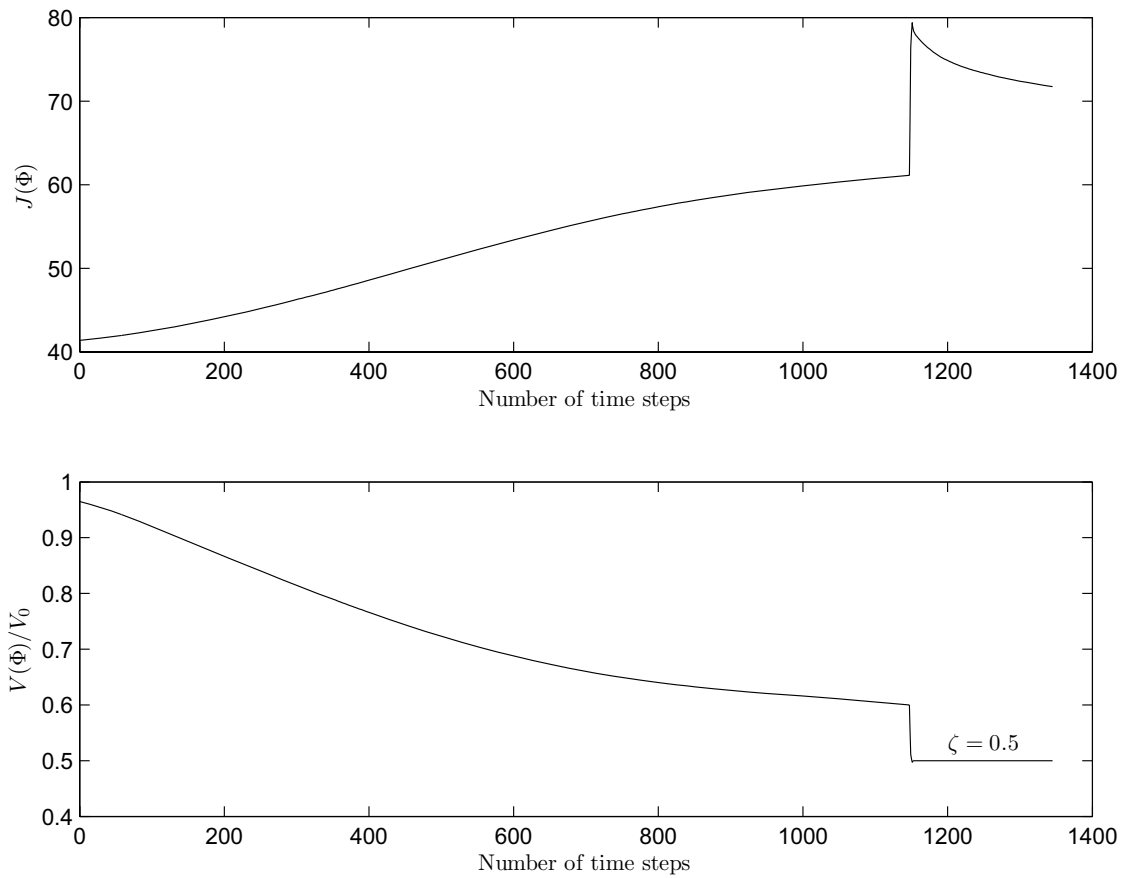


Figure 22: Convergence of the objective and volume functions for the cantilever starting with an initial design with a single hole using a standard level set method.

design with a higher objective function value of 59.617 is different from the one with a lower objective function value of 58.870, as shown in Fig. 14(f). Hence, only a sub-optimal solution is obtained for this case. This is not strange since the present steepest gradient-based local optimization method is still dependent on the initial guess [Bendsøe and Sigmund (2003)] and the ability of the present method to create new holes cannot totally eliminate this dependence. The convergence history of both the objective and constraint functions is shown in Fig. 24. It can be seen that the objective function decreases while new holes are created in the material domain. The present nucleation mechanism can be justified. Rapid convergence can be obtained due to the use of a relatively large timestep and thus the computational efficiency can be improved significantly. The volume constraint can be almost exactly satisfied after the first few timesteps due to the use of the present volume constraint handling approach.

The design without a hole as shown in Fig. 23(a) is further investigated using the standard level set method as aforementioned and Fig. 25 shows the evolution history of the final design. It can be seen that nucleation of new holes is not allowed for and the final design cannot have a hole due to the lack of a nucleation mechanism in the standard level set methods [Sethian (1999); Osher and Fedkiw (2002); Wang, Wang, and Guo (2003); Allaire, de Gournay, Jouve, and Toader (2005)]. The convergence history of both the objective and constraint functions is shown in Fig. 26. The convergence speed of the objective function is significantly slower than the one using the present level set method, as shown in Fig. 24, due to the CFL condition for stability in the standard level set method. The final design converges to a local optimum with an objective function value of 80.125 due to its strong dependence on the initial designs. Hence, compared with the present BIBO time-stable meshfree level set method, the standard level set method can be quite inefficient for simultaneous shape and topology optimization.

5 Conclusions

An unconditionally BIBO time-stable meshfree level set method is presented and applied to structural shape and topology optimization as an accurate and efficient approach. The infinitely smooth inverse multiquadric radial basis functions are used to discretize the implicit level set function to obtain a high level of smoothness and accuracy of the solution to the Hamilton-Jacobi PDE. The original initial value problem is discretized into a time-dependent interpolation problem and the resulting dynamic system of coupled ODEs is positive definite, reinitialization-free and BIBO time-stable because of the present globally supported RBF discretization. Furthermore, a moving superimposed finite element method with adaptive local mesh refinement is adopted to make the physical model consistent with the geometrical model and to achieve a high level of computational accuracy. The present method thus possesses significant advantages in efficiency and accuracy over the standard finite difference-based level set methods. The present level set method is further implemented in the framework of structural shape and topology optimization. An explicit volume constraint handling approach is presented to resolve the volume constraint accurately. The total volume can become conservative and the final design is guaranteed to be feasible. Since reinitialization is eliminated, a physically meaningful nucleation mechanism is established and creation of new holes can be allowed for at the sites where the material is ineffectively used. The final solution becomes less sensitive to the initial design and the probability of converging to a local minimum is greatly reduced. Due to the simultaneous shape and topology optimization, the material domain of the final design will agree well with the region with non-negative extension velocities and an almost homogeneous energy distribution can be achieved. The present method is finally applied to 2D shape and topology optimization of minimum compliance design. Numerical examples can illustrate the superior performance of the present method in accuracy, efficiency, convergence and insensitivity to initial designs over a standard level set method. It is suggested that

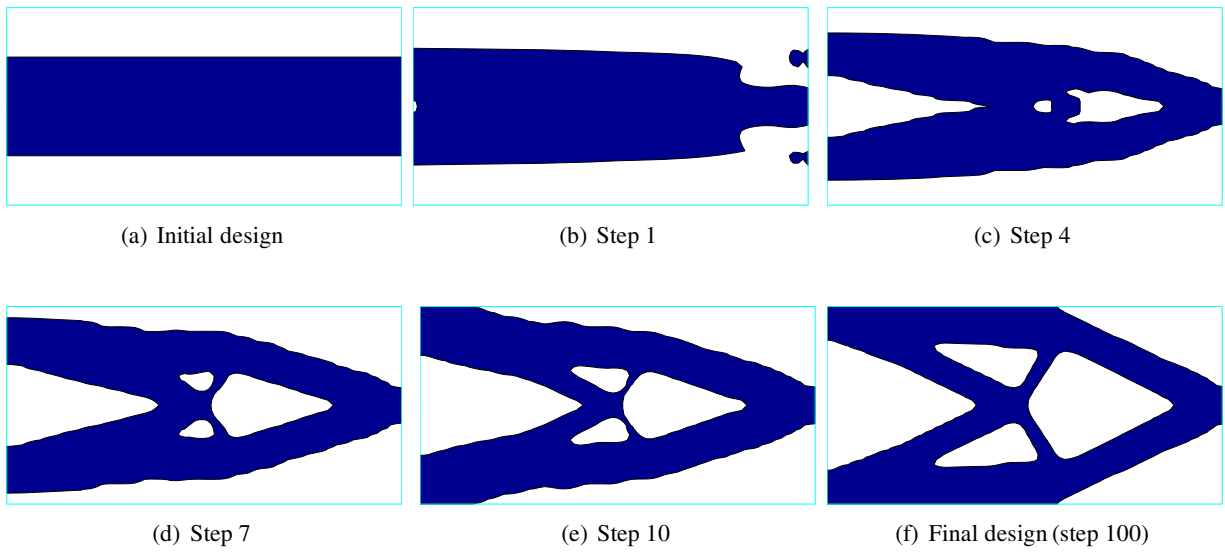


Figure 23: Evolution of the optimal design for the cantilever starting with an initial design without a hole using the present level set method.

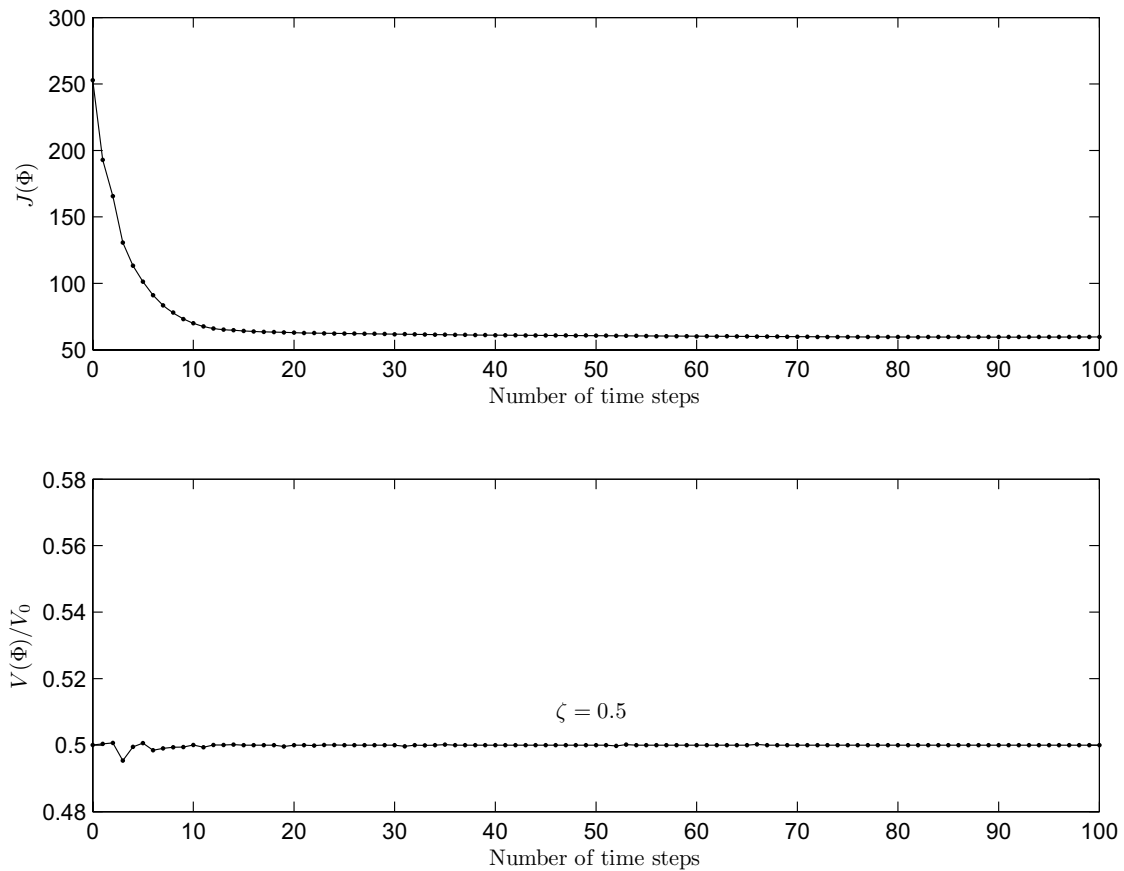


Figure 24: Convergence of the objective and volume functions for the cantilever starting with an initial design without a hole using the present level set method.

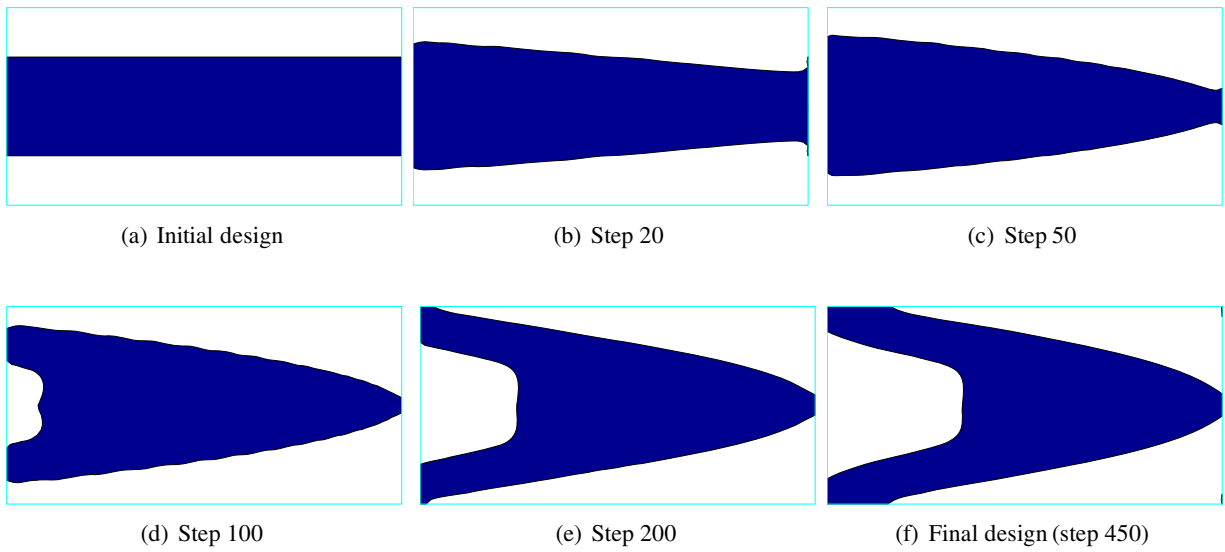


Figure 25: Evolution of the optimal design for the cantilever starting with an initial design without a hole using a standard level set method.

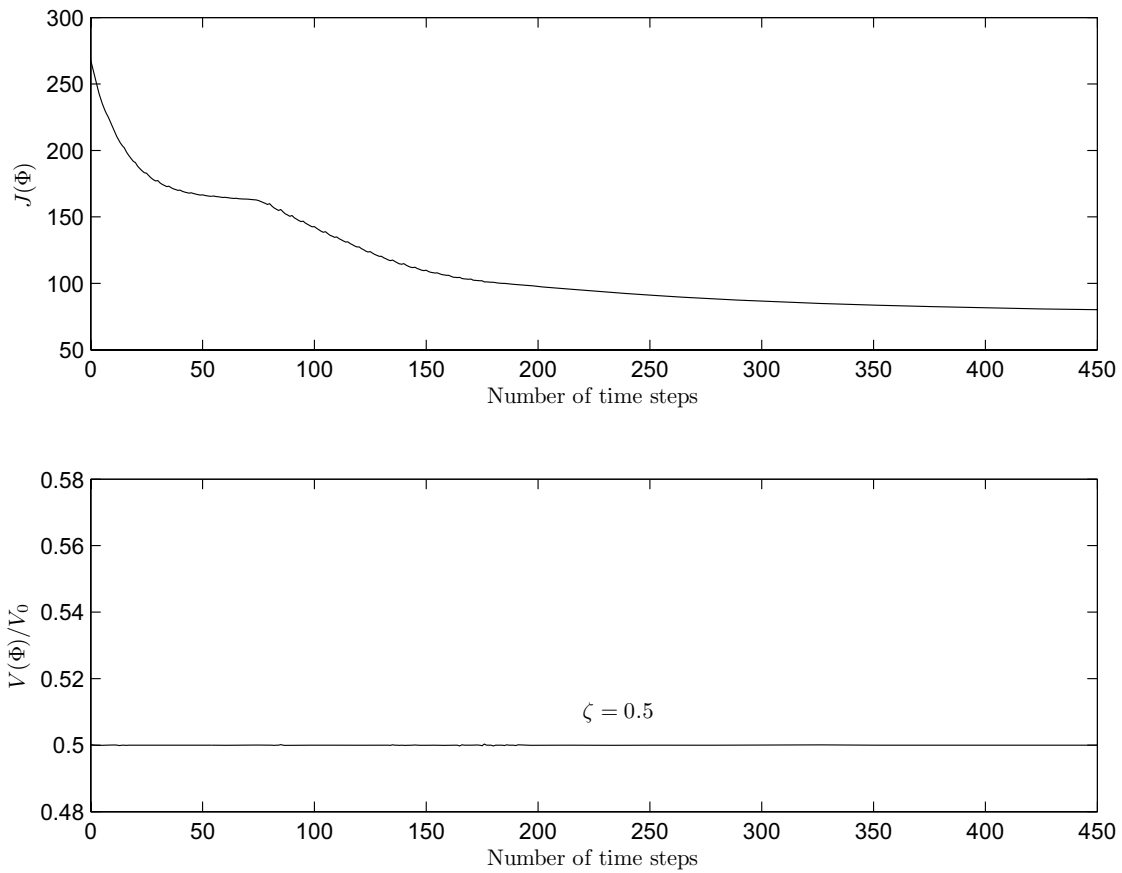


Figure 26: Convergence of the objective and volume functions for the cantilever starting with an initial design without a hole using a standard level set method.

the present level set method is an effective alternative for simultaneous shape and topology optimization.

References

- Akin, J. E.; Arjona-Baez, J.** (2001): Enhancing structural topology optimization. *Engineering Computations*, vol. 18, no. 3–4, pp. 663–675.
- Allaire, G.** (2001): *Shape Optimization by the Homogenization Method*. Springer, New York.
- Allaire, G.; de Gournay, F.; Jouve, F.; Toader, A. M.** (2005): Structural optimization using topological and shape sensitivity via a level set method. *Control and Cybernetics*, vol. 34, no. 1, pp. 59–80.
- Allaire, G.; Gournay, F. D.; Jouve, F.; Toader, A.-M.** (2004): Structural optimization using topological and shape sensitivity via a level set method. Internal report 555, Ecole Polytechnique, France, 2004.
- Allaire, G.; Jouve, F.** (2005): A level set method for vibration and multiple loads structural optimization. *Computer methods in Applied Mechanics and Engineering*, vol. 194, pp. 3269–3290.
- Allaire, G.; Jouve, F.; Toader, A.-M.** (2002): A level-set method for shape optimization. *C. R. Acad. Sci. Paris, Serie I*, vol. 334, pp. 1125–1130.
- Allaire, G.; Jouve, F.; Toader, A.-M.** (2004): Structural optimization using sensitivity analysis and a level-set method. *Journal of Computational Physics*, vol. 194, pp. 363–393.
- Amstutz, S.; Andrä, H.** (2006): A new algorithm for topology optimization using a level-set method. *Journal of Computational Physics*, vol. 216, pp. 573–588.
- Belytschko, T.; Xiao, S. P.; Parimi, C.** (2003): Topology optimization with implicit functions and regularization. *International Journal for Numerical Methods in Engineering*, vol. 57, no. 8, pp. 1177–1196.
- Bendsøe, M. P.** (1989): Optimal shape design as a material distribution problem. *Structural Optimization*, vol. 1, pp. 193–202.
- Bendsøe, M. P.** (1995): *Optimization of structural topology, shape and material*. Springer, Berlin, Heidelberg, New York.
- Bendsøe, M. P.; Kikuchi, N.** (1988): Generating optimal topologies in structural design using a homogenization method. *Computer Methods in Applied Mechanics and Engineering*, vol. 71, pp. 197–224.
- Bendsøe, M. P.; Sigmund, O.** (2003): *Topology Optimization: Theory, Methods and Applications*. Springer-Verlag, Berlin.
- Bhatia, N. P.; Szego, G. P.** (1970): *Stability Theory of Dynamical Systems*. Springer-Verlag, New York.
- Buhmann, M. D.** (2004): *Radial Basis Functions: Theory and Implementations*, volume 12 of *Cambridge Monographs on Applied and Computational Mathematics*. Cambridge University Press, New York, NY.
- Burger, M.** (2004): Lecture notes on infinite-dimensional optimization and optimal design. Report 285J, University of California, Los Angeles, CA, USA, 2004.
- Burger, M.; Hackl, B.; Ring, W.** (2004): Incorporating topological derivatives into level set methods. *Journal of Computational Physics*, vol. 194, pp. 344–362.
- Cecil, T.; Qian, J. L.; Osher, S.** (2004): Numerical methods for high dimensional Hamilton-Jacobi equations using radial basis functions. *Journal of Computational Physics*, vol. 196, no. 1, pp. 327–347.
- Chen, S. K.; Wang, M. Y.; Wang, S. Y.; Xia, Q.** (2005): Optimal synthesis of compliant mechanisms using a connectivity preserving level set method. In *ASME Proceedings of IDETC/CIE 2005*, pp. DETC2005–84748, Long Beach, California, USA.

- Cheng, A.-D.; Golberg, M. A.; Kansa, E. J.; Zammito, G.** (2003): Exponential convergence and H-c multiquadric collocation method for partial differential equations. *Numerical Methods for Partial Equations*, vol. 19, no. 5, pp. 571–594.
- Choi, I.; Horgan, C. O.** (1977): Saint Venant's principle and end effects in anisotropic elasticity. *Journal of Applied Mechanics*, vol. 44, pp. 420–430.
- Cisilino, A. P.** (2007): Topology optimization of 2D potential problems using boundary elements. *CMES: Computer Modeling in Engineering & Sciences*, vol. 15, no. 2, pp. 99–106.
- Eschenauer, H. A.; Kobelev, V. V.; Schumacher, A.** (1994): Bubble method for topology and shape optimization of structures. *Structural Optimization*, vol. 8, no. 1, pp. 42–51.
- Fish, J.; Guttal, R.** (1996): The s-version of finite element method for laminated composites. *International Journal for Numerical Methods in Engineering*, vol. 39, pp. 3641–3662.
- Greenberg, M. D.** (1998): *Advanced Engineering Mathematics*. Prentice-hall International, Inc., Upper Saddle River, New Jersey, USA, 2nd edition.
- Guo, X.; Zhao, K.; Wang, M. Y.** (2005): A new approach for simultaneous shape and topology optimization based on dynamic implicit surface function. *Control and Cybernetics*, vol. 34, no. 1, pp. 255–282.
- Haber, E.** (2004): A multilevel, level-set method for optimizing eigenvalues in shape design problems. *Journal of Computational Physics*, vol. 198, pp. 518–534.
- Hintermuller, M.** (2005): Fast level set based algorithms using shape and topological sensitivity information. *Control and Cybernetics*, vol. 34, no. 1, pp. 305–324.
- Kansa, E. J.; Powerb, H.; Fasshauerc, G. E.; Ling, L.** (2004): A volumetric integral radial basis function method for time-dependent partial differential equations. I. Formulation. *Engineering Analysis with Boundary Elements*, vol. 28, pp. 1191–1206.
- Leito, A.; Scherzer, O.** (2003): On the relation between constraint regularization, level sets, and shape optimization. *Inverse Problems*, vol. 19, no. 1, pp. 1–11.
- Li, C.; Xu, C.; Gu, C.; Fox, M. D.** (2005): Level set evolution without re-initialization: A new variational formulation. In *IEEE International Conference on Computer Vision and Pattern Recognition (CVPR)*, pp. 430–436, San Diego.
- Madsen, N. K.** (1975): The method of lines for the numerical solution of partial differential equations. *ACM SIGNUM Newsletter*, vol. 10, no. 4, pp. 5–7.
- Mallad, R.; Sethian, J. A.; Vemuri, B. C.** (1996): A fast level set based algorithm for topology-independent shape modeling. *Journal of Mathematical Imaging and Vision*, vol. 6, no. 2/3, pp. 269–290.
- Marchandise, E.; Remacle, J.-F.; Chevaugnon, N.** (2006): A quadrature-free discontinuous Galerkin method for the level set equation. *Journal of Computational Physics*, vol. 212, pp. 338–357.
- Micchelli, C. A.** (1986): Interpolation of scattered data: Distance matrices and conditionally positive definite. *Constructive Approximation*, vol. 2, pp. 11–22.
- Michell, A. G. M.** (1904): The limits of economy of material in frame-structures. *Philosophical Magazine*, vol. 8, no. 6, pp. 589–597.
- Mitchell, I. M.** (2004): A toolbox of level set methods. Tech. Rep. TR-2004-09, Department of Computer Science, University of British Columbia, Canada, 2004.
- Morse, B. S.; Yoo, T. S.; Chen, D. T.; Rheingans, P.; Subramanian, K. R.** (2001): Interpolating implicit surfaces from scattered surface

data using compactly supported radial basis functions. In *SMI '01: Proceedings of the International Conference on Shape Modeling & Applications*, pp. 89–98, Washington, DC, USA. IEEE Computer Society.

Norato, J.; Haber, R.; Tortorelli, D.; Bendsøe, M. P. (2004): A geometry projection method for shape optimization. *International Journal for Numerical Methods in Engineering*, vol. 60, no. 14, pp. 2289–2312.

Okada, H.; Liu, C. T.; Ninomiya, T.; Fukui, Y.; Kumazara, N. (2004): Analysis of particulate composite materials using an element overlay technique. *CMES: Computer Modeling in Engineering & Sciences*, vol. 6, no. 4, pp. 333–347.

Osher, S.; Fedkiw, R. P. (2001): Level set methods: An overview and some recent results. *Journal of Computational Physics*, vol. 169, pp. 463–502.

Osher, S.; Paragios, N. (2003): *Geometric Level Set Methods in Imaging, Vision, and Graphics*. Springer-Verlag, New York.

Osher, S.; Santosa, F. (2001): Level-set methods for optimization problems involving geometry and constraints: Frequencies of a two-density inhomogeneous drum. *Journal of Computational Physics*, vol. 171, pp. 272–288.

Osher, S.; Sethian, J. A. (1988): Front propagating with curvature dependent speed: Algorithms based on Hamilton-Jacobi formulations. *Journal of Computational Physics*, vol. 78, pp. 12–49.

Osher, S. J.; Fedkiw, R. P. (2002): *Level Set Methods and Dynamic Implicit Surfaces*. Springer-Verlag, New York.

Paris, J.; Casteleiro, M.; Navarrina, F.; Colominas, I. (2007): Topology optimization of structures with local and global stress constraints. In *ICCES*, volume 2 of 1, pp. 13–19.

Peng, D.; Merriman, B.; Osher, S.; Zhao, H.; Kang, M. (1999): A PDE-based fast local level set method. *Journal of Computational Physics*, vol. 155, pp. 410–438.

Platte, R. B.; Driscoll, T. A. (2005): Eigenvalue stability of radial basis function discretizations for time-dependent problems. Technical Report 2005–01, Department of Mathematical Sciences, University of Delaware, USA, 2005.

Rozvany, G. (1998): *Structural Design via Optimality Criteria*. Kluwer, Dordrecht.

Rozvany, G. I. N. (2001): Aims, scope, methods, history and unified terminology of computer-aided topology optimization in structural mechanics. *Structural and Multidisciplinary Optimization*, vol. 21, no. 2, pp. 90–108.

Rozvany, G. I. N. (2001): Stress ratio and compliance based methods in topology optimization - A critical review. *Structural and Multidisciplinary Optimization*, vol. 21, pp. 109–119.

Rozvany, G. I. N.; Zhou, M.; Birker, T. (1992): Generalized shape optimization without homogenization. *Structural Optimization*, vol. 4, pp. 250–254.

Schaback, R.; Wendland, H. (2001): Characterization and construction of radial basis functions. In Dyn, N.; Leviatan, D.; Levin, D.; Pinkus, A.(Eds): *Multivariate approximation and applications*, pp. 1–24. Cambridge University Press, Cambridge, UK.

Sethian, J. A. (1999): *Level Set Methods and Fast Marching Methods*. Cambridge Monographs on Applied and Computational Mathematics. Cambridge University Press, Cambridge, UK, 2nd edition.

Sethian, J. A.; Wiegmann, A. (2000): Structural boundary design via level set and immersed interface methods. *Journal of Computational Physics*, vol. 163, no. 2, pp. 489–528.

Sigmund, O. (2001): A 99 line topology optimization code written in MATLAB. *Structural and Multidisciplinary Optimization*, vol. 21, no. 2, pp. 120–127.

Sokolowski, J.; Żochowski, A. (2001): Topological derivatives of shape functionals for elasticity systems. *Mechanics of Structures and Machines*, vol. 29, no. 3, pp. 331–349.

Sokolowski, J.; Zolesio, J.-P. (1992): Introduction to shape optimization: shape sensitivity analysis. In *Springer Series in Computational Mathematics*, volume 10. Springer, Berlin, Germany.

Tapp, C.; Hansel, W.; Mittelstedt, C.; Becker, W. (2004): Weight-minimization of sandwich structures by a heuristic topology optimization algorithm. *CMES: Computer Modeling in Engineering & Sciences*, vol. 5, no. 6, pp. 563–574.

Tsai, R.; Osher, S. (2003): Level set methods and their applications in image science. *Communications in Mathematical Sciences*, vol. 1, no. 4, pp. 623–656.

van den Doel, K.; Ascher, U. (2006): On level set regularization for highly ill-posed distributed parameter estimation problems. *Journal of Computational Physics*, vol. 216, no. 2, pp. 707–723.

Wang, M. Y.; Chen, S.; Wang, X.; Mei, Y. (2005): Design of multimaterial compliant mechanisms using level-set methods. *ASME Journal of Mechanical Design*, vol. 127, pp. 941–956.

Wang, M. Y.; Wang, S. Y. (2005): Bilateral filtering for structural topology optimization. *International Journal for Numerical Methods in Engineering*, vol. 63, no. 13, pp. 1911–1938.

Wang, M. Y.; Wang, X. (2004): PDE-driven level sets, shape sensitivity and curvature flow for structural topology optimization. *CMES: Computer Modeling in Engineering & Sciences*, vol. 6, no. 4, pp. 373–396.

Wang, M. Y.; Wang, X. (2005): A level-set based variational method for design and optimization of heterogeneous objects. *Computer-Aided Design*, vol. 37, pp. 321–337.

Wang, M. Y.; Wang, X.; Guo, D. (2003): A level set method for structural topology optimization. *Computer Methods in Applied Mechanics and Engineering*, vol. 192, pp. 227–246.

Wang, M. Y.; Wang, X.; Guo, D. (2004): Structural shape and topology optimization in a level

set method based framework of region representation. *Structural and Multidisciplinary Optimization*, vol. 27, pp. 1–19.

Wang, M. Y.; Wang, X. M. (2004): “Color” level sets: A multi-phase method for structural topology optimization with multiple materials. *Computer Methods in Applied Mechanics and Engineering*, vol. 193, no. 6–8, pp. 469–496.

Wang, M. Y.; Zhou, S. (2004): Phase field: A variational method for structural topology optimization. *CMES: Computer Modeling in Engineering & Sciences*, vol. 6, no. 6, pp. 547–566.

Wang, S. Y.; Lim, K. M.; Khoo, B. C.; Wang, M. Y. (2007): An extended level set method for shape and topology optimization. *Journal of Computational Physics*, vol. 221, no. 1, pp. 395–421.

Wang, S. Y.; Tai, K. (2004): Graph representation for evolutionary structural topology optimization. *Computers & Structures*, vol. 82, no. 20–21, pp. 1609–1622.

Wang, S. Y.; Tai, K. (2005): Bar-system representation method for structural topology optimization using the genetic algorithms. *Engineering Computations*, vol. 22, no. 2, pp. 206–231.

Wang, S. Y.; Tai, K.; Quek, S. T. (2006): Topology optimization of piezoelectric sensors/actuators for torsional vibration control of composite plates. *Smart Materials and Structures*, vol. 15, pp. 253–269.

Wang, S. Y.; Tai, K.; Wang, M. Y. (2006): An enhanced genetic algorithm for structural topology optimization. *International Journal for Numerical Methods in Engineering*, vol. 65, no. 1, pp. 18–44.

Wang, S. Y.; Wang, M. Y. (2006): A moving superimposed finite element method for structural topology optimization. *International Journal for Numerical Methods in Engineering*, vol. 65, no. 11, pp. 1892–1922.

Wang, S. Y.; Wang, M. Y. (2006): Radial basis functions and level set method for structural

topology optimization. *International Journal for Numerical Methods in Engineering*, vol. 65, no. 12, pp. 2060–2090.

Wang, S. Y.; Wang, M. Y. (2006): Structural shape and topology optimization using an implicit free boundary parametrization method. *CMES: Computer Modeling in Engineering & Sciences*, vol. 13, no. 2, pp. 119–147.

Wang, X.; Mei, Y.; Wang, M. Y. (2004): Incorporating topology/phase derivatives into level set methods for optimization of solids. In *WISDOM 2004-Warsaw International Seminar on Design and Optimal Modeling*, Warsaw, Poland.

Xie, Y. M.; Steven, G. P. (1993): A simple evolutionary procedure for structural optimization. *Computers & Structures*, vol. 49, no. 5, pp. 885–896.

Ye, J. C.; Bresler, Y.; Moulin, P. (2002): A self-referencing level-set method for image reconstruction from sparse Fourier samples. *International Journal of Computer Vision*, vol. 50, no. 3, pp. 253–270.

Zhou, M.; Rozvany, G. I. N. (2001): On the validity of ESO type methods in topology optimization. *Structural and Multidisciplinary Optimization*, vol. 21, no. 1, pp. 80–83.

Zhou, S.; Wang, M. Y. (2006): 3D multi-material structural topology optimization with the generalized Cahn-Hilliard equations. *CMES: Computer Modeling in Engineering & Sciences*, vol. 16, no. 2, pp. 83–102.